III. 学会等発表実績

学 会 等 発 表 実 績

委託業務題目「ＭＹＣＮ遺伝子塩基配列特異的アルキル化による進行神経芽腫に対する新規薬剤開発に関する研究」

機関名　千葉県がんセンター研究所

１．学会等における口頭・ポスター発表

発表した成果（発表題目、口頭・ポスター発表の別）	発表者氏名	発表した場所（学会等名）	発表した時期	国内・外の別
Efficient Gene Silencing by PI Polyamide with Aliphatic/Aromatic Amino Acid Pairings Targeting MMP-9	T.Watanabe, N.Koshikawa, T.Ozaki, T.Bando, H.Sugiyama,H.Nagase	日本癌学会学術総会	2014年9月25日-27日	国内
Targeting specific DNA sequences by N-methylpyrrole and N-methylimidazole polyamides provides insights for the development of novel diagnostic and therapeutic drugs.	Takatori A, Yoda H, Hiraoka K, Shinohara K, Watanabe T, Koshikawa N, Nagase H.	The 28th International Mammalian Genome Conference	2014年10月26日-29日	国外

２．学会誌・雑誌等における論文掲載

掲載した論文（発表題目）	発表者氏名	発表した場所（学会誌・雑誌等名）	発表した時期	国内・外の別
Identification of a novel E-box binding pyrrole-imidazole polyamide inhibiting MYC-driven cell proliferation.	Mishra R, Watanabe T, Kimura MT, Koshikawa N, Ikeda M, Uekusa S, Kawashima H, Wang X, Igarashi J, Choudhury D, Grandori C, Kemp CJ, Ohira M, Verma NK, Kobayashi Y, Takeuchi J, Koshinaga T, Nemoto N, Fukuda N, Soma M, Kusafuka T, Fujiwara K, Nagase H.	Cancer Sci.	2015	国外
Intracellular fragment of NLRR3 (NLRR3-ICD) stimulates ATRA-dependent neuroblastoma differentiation.	Akter J, Takatori A*, Islam MS, Nakazawa A, Ozaki T, Nagase H, Nakagawara A. (*Corresponding author)	Biochem. Biophys. Res. Commun.	2014	国外

Ⅳ．研究成果の刊行物・別刷

Biochemical and Biophysical Research Communications 453 (2014) 86–93

Contents lists available at ScienceDirect

Biochemical and Biophysical Research Communications

journal homepage: www.elsevier.com/locate/ybbrc

Intracellular fragment of NLRR3 (NLRR3-ICD) stimulates ATRA-dependent neuroblastoma differentiation

Jesmin Akter [a], Atsushi Takatori [b,*], Md. Sazzadul Islam [a], Atsuko Nakazawa [c], Toshinori Ozaki [d,*], Hiroki Nagase [b], Akira Nakagawara [e]

[a] Laboratory of Innovative Cancer Therapeutics, Chiba Cancer Center Research Institute, Chiba 260-8717, Japan
[b] Laboratory of Cancer Genetics, Chiba Cancer Center Research Institute, Chiba 260-8717, Japan
[c] Department of Pathology, National Center for Child Health and Development, Tokyo, Japan
[d] Laboratory of DNA Damage Signaling, Chiba Cancer Center Research Institute, Chiba 260-8717, Japan
[e] Saga Medical Centre, 840-8571, Japan

ARTICLE INFO

Article history:
Received 13 September 2014
Available online 23 September 2014

Keywords:
ATRA
Differentiation
Neuroblastoma
NLRR3
Secretase

ABSTRACT

We have previously identified neuronal leucine-rich repeat protein-3 (NLRR3) gene which is preferentially expressed in favorable human neuroblastomas as compared with unfavorable ones. In this study, we have found for the first time that NLRR3 is proteolytically processed by secretases and its intracellular domain (NLRR3-ICD) is then released to translocate into cell nucleus during ATRA-mediated neuroblastoma differentiation. According to our present observations, NLRR3-ICD was induced to accumulate in cell nucleus of neuroblastoma SH-SY5Y cells following ATRA treatment. Since the proteolytic cleavage of NLRR3 was blocked by α- or γ-secretase inhibitor, it is likely that NLRR3-ICD is produced through the secretase-mediated processing of NLRR3. Intriguingly, forced expression of NLRR3-ICD in neuroblastoma SK-N-BE cells significantly suppressed their proliferation as examined by a live-cell imaging system and colony formation assay. Similar results were also obtained in neuroblastoma TGW cells. Furthermore, overexpression of NLRR3-ICD stimulated ATRA-dependent neurite elongation in SK-N-BE cells. Together, our present results strongly suggest that NLRR3-ICD produced by the secretase-mediated proteolytic processing of NLRR3 plays a crucial role in ATRA-mediated neuronal differentiation, and provide a clue to develop a novel therapeutic strategy against aggressive neuroblastomas.

1. Introduction

Neuroblastoma which originates from the sympathetic nervous system during embryogenesis, is the most common extra cranial solid tumor in children, accounting for 15% of childhood cancer deaths [1]. Neuroblastoma is highly heterogeneous, and thus characterized by a wide variety of its clinical behaviors, from spontaneous regression to aggressive progression. For example, tumors found in infants less than 1 year of age frequently regress through the spontaneous differentiation and/or apoptosis, resulting in a favorable prognosis [2]. It has been shown that neuroblastoma cells with better prognosis are often found to express various prognostic markers indicative of cell differentiation, such as *HNK-1* or *TrkA* [3,4]. On the other hand, around 40% of the patients diagnosed with neuroblastoma are included in the high-risk category based on prognostic indicators such as age at diagnosis, stage, tumor histology, proto-oncogene *MYCN* status, and DNA ploidy [5,6]. Among them, the poor clinical outcome and aggressive tumor phenotype of high-risk neuroblastoma strongly correlate with the amplification of *MYCN* and enhanced tumor angiogenesis [7]. Although patients with the high-risk tumors usually have a good immediate response to the standard treatment, the majority of them frequently acquire resistance to the therapy with fatal outcome [1]. Therefore, a novel strategy to treat these advanced tumors is highly required.

Intriguingly, neuroblastoma cells display the similar characteristics to undifferentiated cells [8], indicating that the tumorigenesis of neuroblastoma results from defect in differentiation of embryonic neural crest progenitor cells [9]. With this in mind, a growing body of evidence strongly suggests that neuroblastoma cells have an ability to differentiate into mature cells and can be

* Corresponding authors at: Laboratory of Cancer Genetics, Chiba Cancer Center Research Institute, 666-2 Nitona, Chuoh-ku, Chiba 260-8717, Japan. Fax: +81 43 265 4459 (A. Takatori). Laboratory of DNA Damage Signaling, Chiba Cancer Center Research Institute, 666-2 Nitona, Chuoh-ku, Chiba 260-8717, Japan. Fax: +81 43 265 4459 (T. Ozaki).
E-mail addresses: atakatori@chiba-cc.jp (A. Takatori), tozaki@chiba-cc.jp (T. Ozaki).

http://dx.doi.org/10.1016/j.bbrc.2014.09.065
0006-291X/

forced to differentiate in response to retinoic acid (RA) [10]. RA has been shown to play an important role in early embryonic development and in the generation of several systems such as nervous system [11]. Based on these findings, RA-mediated terminal differentiation of neuroblastoma is used as a current standard therapy for the high-risk neuroblastoma, however, a precise molecular basis underlying neuroblastoma differentiation has been elusive.

To understand a molecular mechanism(s) behind the genesis as well as the aggressive progression of neuroblastoma, we have identified a large number of genes expressed differentially between favorable and unfavorable neuroblastomas [12]. NLRR3 is one of NLRR family of type I transmembrane protein with the typical leucine-rich repeat (LRR) domain, and its expression level was extremely higher in favorable neuroblastomas than that in unfavorable ones, indicating that *NLRR3* expression might be one of favorable prognostic indicators in neuroblastoma [12,13]. Recently, we have found that MYCN has an ability to repress the transcription of *NLRR3* through the functional collaboration with Miz-1, raising a possibility that MYCN-induced down-regulation of NLRR3 contributes at least in part to the aggressive phenotype of the high-risk neuroblastoma [14]. However, the precise molecular event(s) and mechanism(s) involved remain unclear.

In this study, we have found that the intracellular fragment of NLRR3 (NLRR3-ICD) plays a pivotal role in the regulation of ATRA (all-*trans* retinoic acid)-mediated neuroblastoma differentiation.

2. Materials and methods

2.1. Cell lines

Human neuroblastoma SK-N-BE, SH-SY5Y and TGW cells were grown in RPMI 1640 medium (Sigma) supplemented with 10% heat-inactivated fetal bovine serum (Invitrogen), 100 units/ml of penicillin and 100 μg/ml of streptomycin. Cells were grown at 37 °C in a humidified incubator with 5% CO_2. For neuroblastoma differentiation experiments, SH-SY5Y cells were exposed to 5 μM of all-*trans* retinoic acid (ATRA; Sigma).

2.2. Clinical samples

Patient samples were collected with patients' written informed consent in accordance with ethics approval obtained from the internal review board.

2.3. Transfection

Cells were transfected with the indicated expression plasmids using LipofectAMINE 2000 (Invitrogen) according to the manufacturer's instructions.

2.4. Deletion constructs of NLRR3

The expression plasmids encoding human NLRR3 (1–708), NLRR3-ECD (1–649), NLRR3-ECD-sol (1–628), NLRR3-d-ECD (629–708) or NLRR3-ICD (648–708) were generated by PCR-based amplification. PCR products were gel-purified and inserted into the appropriate restriction sites of pcDNA3.1 expression plasmid (Invitrogen) with COOH-terminal HA epitope tag to give pcDNA3.1-NLRR3, pcDNA3.1-NLRR3-ECD, pcDNA3.1-NLRR3-ECD-sol, pcDNA3.1-NLRR3-d-ECD and pcDNA3.1-NLRR3-ICD. The nucleotide sequences of these expression plasmids were verified by DNA sequencing.

2.5. Cell survival assay

Cells were seeded at a density of 1.0×10^3 cells/96-well plates and allowed to attach overnight. Cells were then maintained in standard culture medium, and visualized using a real-time cell imaging system (IncuCyte; Essen's Bioscience) according to the manufacturer's recommendations.

2.6. Colony formation assay

SK-N-BE or TGW cells were seeded at a density of 2.0×10^3 cells/6-well plates, and then transfected with the indicated expression plasmids. Forty-eight hours after transfection, cells were transferred to the fresh medium containing G418 (600 μg/ml). After 14 days of the incubation, G418-resistant colonies were fixed in methanol, and stained with Giemsa's solution.

2.7. Immunoprecipitation

Equal amounts of cell lysates (1 mg of protein) were precleared with 20 μl of protein A-Sepharose beads (GE Healthcare) and subjected to immunoprecipitation with anti-NLRR3 or with anti-HA antibody (Roche). The immunoprecipitates were then analyzed by immunoblotting with anti-NLRR3 or with anti-HA antibody. ECL (enhanced chemiluminescence; GE Healthcare) was used to detect the presence of immuno-reactive bands.

2.8. Immunohistochemistry

Paraffin-embedded sympathetic ganglia tissues were fixed in 10% formaldehyde and then incubated with anti-NLRR3 antibody. Immunohistochemical analysis was performed as described [14].

2.9. Immunofluorescence

Cells were grown on glass coverslips in standard culture medium. Cells were washed in PBS, fixed in 4% paraformaldehyde for 20 min at 4 °C, permeabilized with 0.1% Triton X-100 for 20 min at room temperature, and then blocked with 1% BSA plus 5% goat serum for 1 h at room temperature. After blocking, cells were incubated with anti-HA, anti-NLRR3, anti-Tuj-1 antibody (Covance) or with a normal rabbit IgG for 1 h at room temperature, followed by the incubation with Alexa Fluor 546-conjugated goat anti-rabbit IgG (Life Technologies). Cell nuclei were stained with DAPI. The coverslips were mounted into glass slides, and images were captured using a confocal laser scanning microscope (Leica).

2.10. Statistical analysis

All values were expressed as the means ± SEM. One-way ANOVA with a post hoc Dunnett's test were used to determine level of significance for colony formation assay and percentage of differentiated cells ($^{**}P < 0.01$). Two-way ANOVA followed by a multiple comparison post hoc Bonferroni's test was used to compare differences between groups in cell viability assay ($^{*}P < 0.05$ and $^{**}P < 0.01$).

3. Results

3.1. Induction of NLRR3-related peptide during ATRA-mediated neuroblastoma differentiation

To examine the expression pattern of NLRR3 during ATRA (all-*trans* retinoic acid)-dependent neuroblastoma differentiation, human neuroblastoma SH-SY5Y cells were exposed to 5 μM of

ATRA. At the indicated time periods after treatment, cell lysates were subjected to immunoprecipitation/immunoblotting with anti-NLRR3 antibody. Consistent with our recent findings [14], an obvious elongation of neurite (one of the hallmark processes of neuronal morphological differentiation) was observed in ATRA-treated SH-SY5Y cells in a time-dependent manner (Fig. 1A). It is worth noting that ATRA promotes a remarkable accumulation of a small peptide which is recognized by anti-NLRR3 antibody (Fig. 1B).

Since anti-NLRR3 antibody was raised against the extreme COOH-terminal intracellular domain of NLRR3 [14], it is possible that, like NICD (Notch intracellular domain) [15], this small peptide is produced by a proteolytic cleavage of NLRR3 in SH-SY5Y cells exposed to ATRA. It has been well-documented that, upon ligand binding, NICD is released from the plasma membrane after proteolytic processing, and thereby translocating into cell nucleus [15]. To test this possibility, we performed the indirect immunofluorescence experiments to examine the subcellular localization of NLRR3 in response to ATRA. At the indicated time points after ATRA treatment, SH-SY5Y cells were fixed and stained with anti-NLRR3 antibody. As shown in Fig. 1C, NLRR3 was extremely detectable outside of cell nucleus in the absence of ATRA. Intriguingly, a small fraction of NLRR3 was clearly induced to accumulate in ATRA-treated cell nucleus in a time-dependent fashion, suggesting that ATRA-mediated proteolysis releases the intracellular domain of NLRR3 from plasma membrane and thereby promoting its nuclear access. Although further experiments should be required to address this issue, we tentatively termed this small peptide NLRR3-ICD (NLRR3 intracellular domain).

3.2. Secretase-dependent proteolytic cleavage of NLRR3 to generate NLRR3-ICD

It has been widely accepted that NICD is generated through the sequential and highly regulated intramembrane proteolysis mediated by three distinct types of proteases including γ-secretase complex [15]. As described [16], γ-secretase cleaves quite a broad range of substrates, and there are no distinct consensus amino acid sequences of intramembrane γ-cleavage sites among them (Fig. 2A). Considering that NLRR3-ICD might be released from the plasma membrane, it is likely that γ-secretase-mediated proteolytic cleavage is involved in the production of NLRR3-ICD. To verify this hypothesis, we took advantage of γ-secretase inhibitor, inhibitor X [17]. SH-SY5Y cells were treated with inhibitor X or left untreated. Twenty-four hours post treatment, cell lysates were analyzed by immunoprecipitation/immunoblotting with anti-NLRR3 antibody. As shown in Fig. 2B, NLRR3-ICD was undetectable in the presence of inhibitor X, indicating that γ-secretase activity is required for the production of NLRR3-ICD.

To further confirm this issue, neuroblastoma SK-N-BE cells were transfected with the expression plasmid for HA-tagged NLRR3, followed by an incubation with or without inhibitor X. The endogenous expression level of NLRR3 in SK-N-BE cells was quite low when compared with that in SH-SY5Y cells (data not shown).

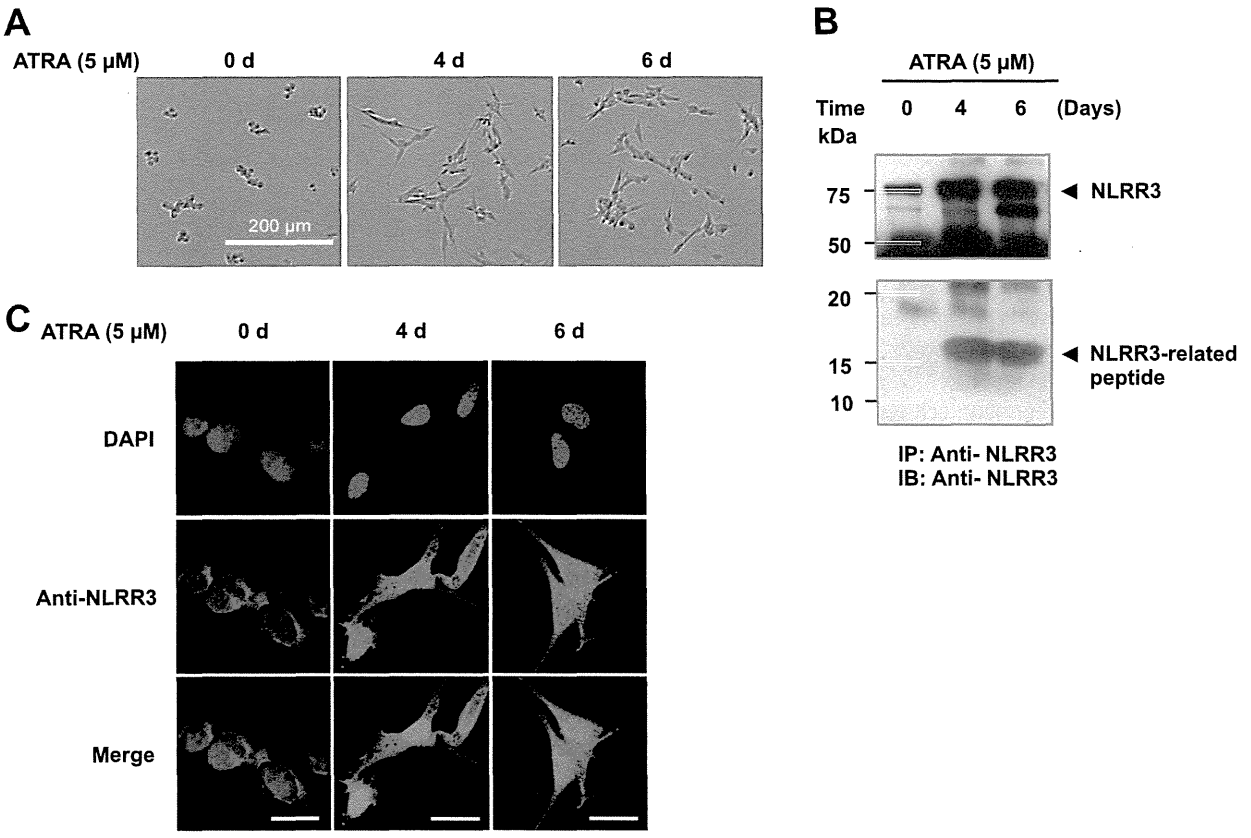

Fig. 1. Accumulation of an NLRR3-related peptide during ATRA-mediated neuroblastoma differentiation. (A) ATRA-mediated neuronal differentiation of neuroblastoma SH-SY5Y cells. SH-SY5Y cells were treated with 5 μM of ATRA. At the indicated time periods after treatment, pictures were taken. Note that ATRA-dependent neurite outgrowth was seen. Scale bar; 200 μm. (B) Expression of NLRR3 in response to ATRA. SH-SY5Y cells were treated as in (A). At the indicated time points after ATRA exposure, cell lysates were analyzed by immunoprecipitation with anti-NLRR3 antibody, followed by immunoblotting with anti-NLRR3 antibody. Arrow heads indicate native NLRR3 and NLRR3-related peptide. (C) ATRA-mediated nuclear access of NLRR3. SH-SY5Y cells were treated as in (A). At the indicated time periods after ATRA treatment, cells were fixed and then probed with anti-NLRR3 antibody, followed by the incubation with Alexa flour 546-conjugated secondary antibody (red). Cells were also stained with DAPI to visualize nuclei (blue). Scale bar; 25 μm. (For interpretation of the references to color in this figure legend, the reader is referred to the web version of this article.)

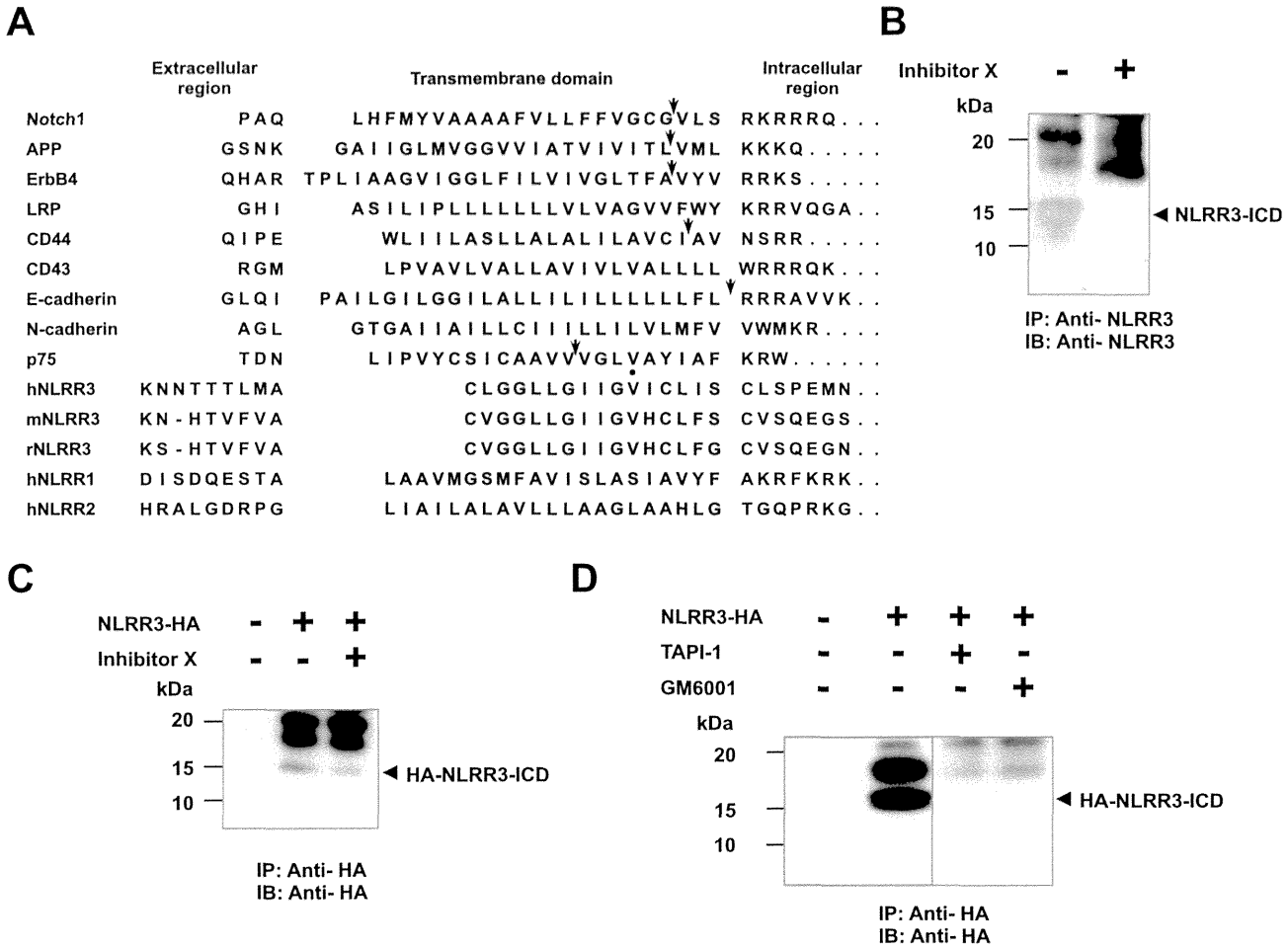

Fig. 2. Production of NLRR3 COOH-terminal peptide (NLRR3-ICD) through the proteolytic cleavage of NLRR3 by α- and γ-secretases. (A) Alignment of the amino acid sequences from transmembrane domains of human γ-secretase substrates. Arrows and filled circle indicate γ-cleavage sites of the indicated substrates and potential γ-cleavage site of NLRR3, respectively. (B and C) γ-secretase inhibitor blocks the production of NLRR3-ICD. SH-SY5Y cells were treated with 1 μM of inhibitor X or left untreated. Twenty-four hours after treatment, cell lysates were immunoprecipitated with anti-NLRR3 antibody, followed by immunoblotting with anti-NLRR3 antibody (B). SK-N-BE cells were transfected with the empty plasmid or with the expression plasmid for HA-NLRR3 and treated with or without inhibitor X. Twenty-four hours after treatment, cell lysates were subjected to immunoprecipitation with anti-HA antibody, followed by immunoblotting with anti-HA antibody (C). (D) The production of NLRR3-ICD is blocked by α-secretase inhibitors. SK-N-BE cells were transfected with the empty plasmid or with the expression plasmid encoding HA-NLRR3, and incubated in the presence or absence of TAPI-1 (20 μM) or GM6001 (10 μM). Twenty-four hours after treatment, cell lysates were processed for immunoprecipitation with anti-HA antibody, followed by immunoblotting with anti-HA antibody.

Twenty-four hours after treatment, cell lysates were analyzed by immunoprecipitation/immunoblotting with anti-HA antibody. As shown in Fig. 2C, the amount of HA-NLRR3-ICD was reduced in cells exposed to inhibitor X. Next, we have introduced the expression plasmid encoding HA-NLRR3 into SK-N-BE cells, and the transfected cells were then exposed to α-secretase inhibitors such as TAPI-1 and GM6001 [18] or left untreated. As clearly seen in Fig. 2D, the generation of HA-NLRR3-ICD was greatly abolished by these inhibitor treatments. Thus, it is highly likely that NLRR3-ICD is produced at least in part through the secretase-dependent proteolytic cleavage of NLRR3.

3.3. Nuclear access of NLRR3-ICD

We next assessed whether NLRR3-ICD could be localized within cell nucleus. SK-N-BE cells were transfected with the expression plasmid for HA-NLRR3. Forty-eight hours post transfection, the transfected cells were biochemically fractionated into cytoplasmic and nuclear fractions, and equal amounts of each fraction were analyzed by immunoblotting with anti-HA antibody. The purity of the cytoplasmic and nuclear fractions were verified by immunoblotting with anti-tubulin-α and anti-lamin B antibodies, respectively. As shown in Fig. 3A, the exogenously expressed HA-NLRR3 underwent proteolytic processing and the resultant HA-NLRR3-ICD was largely detected in nuclear fraction.

To gain further insights into the nuclear distribution of NLRR3-ICD, we have constructed the expression plasmids encoding the indicated HA-NLRR3 deletion mutants (Fig. 3B), and introduced them into SK-N-BE cells. Forty-eight hours after transfection, cells were fixed and probed with anti-HA antibody. As shown in Fig. 3C, HA-NLRR3-ECD and HA-NLRR3-ECD-sol lacking the intracellular domain of NLRR3, exclusively existed outside of cell nucleus, whereas HA-NLRR3-d-ECD containing NLRR3 intracellular domain, was found in both cytoplasm and nucleus. As expected, the nuclear distribution of HA-NLRR3-ICD was observed under our experimental conditions.

Next, we sought to examine whether the nuclear NLRR3 could be also detectable *in vivo*. For this purpose, we have performed an immunohistochemical analysis. Human sympathetic ganglia were fixed in formaldehyde, followed by an incubation with normal rabbit serum or with anti-NLRR3 antibody. As shown in Fig. 3D, anti-NLRR3 antibody recognized the nuclear NLRR3 in sympathetic ganglia, whereas normal rabbit serum did not detect any signals. Together, it appears that NLRR3 is subjected to the

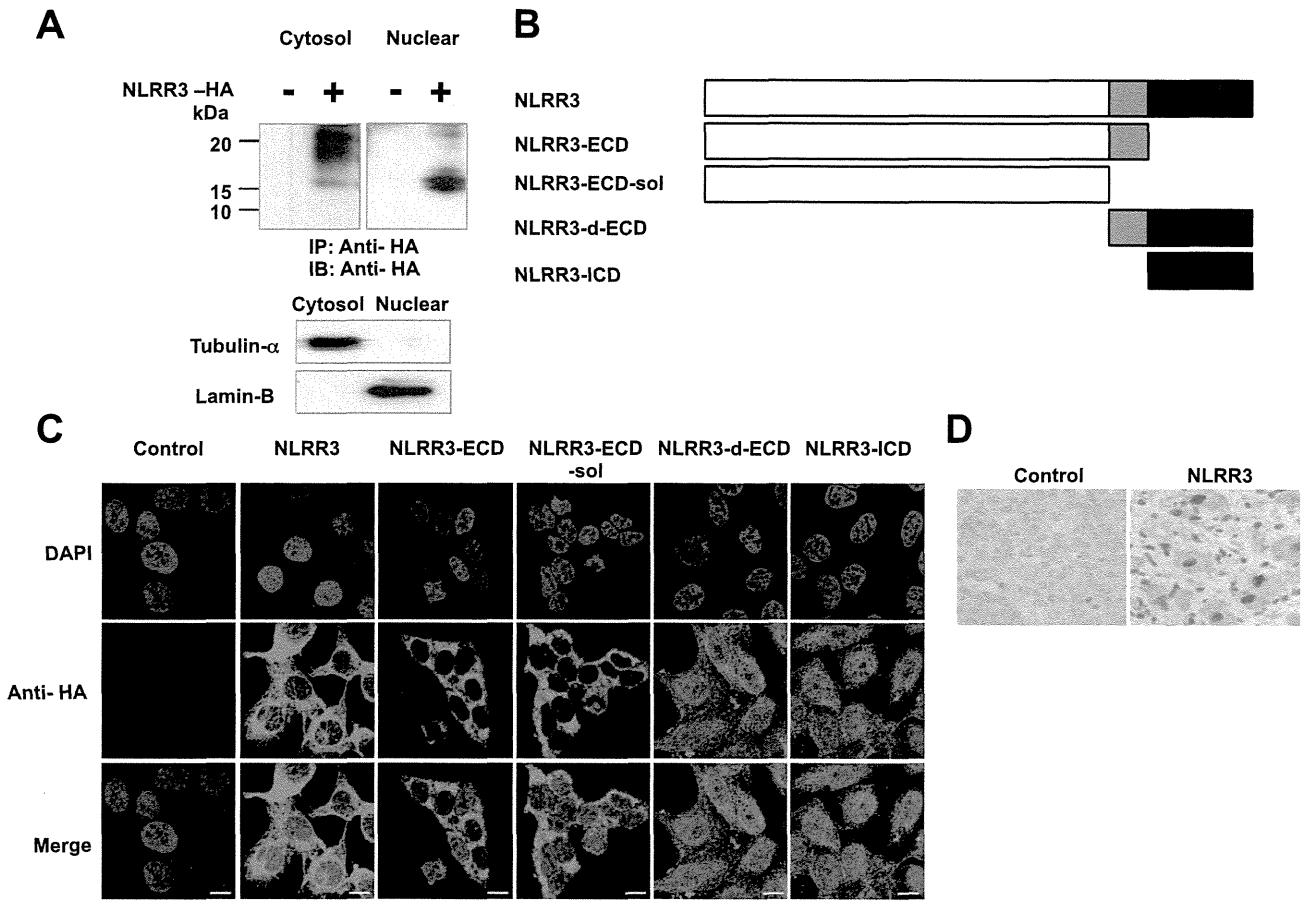

Fig. 3. Nuclear localization of NLRR3-ICD in neuroblastoma cells. (A) Immunoblotting. SK-N-BE cells were transfected with the empty plasmid or with the expression plasmid for HA-NLRR3. Forty-eight hours after transfection, cells were fractionated into cytoplasmic (C) and nuclear (N) fractions. Equal amounts of each fraction were analyzed by immunoblotting with anti-HA (upper panels), anti-Tubulin-α (middle panel), or with anti-Lamin B (lower panel). (B) Schematic diagrams of a full-length NLRR3 and its deletion mutants. Extracellular, transmembrane and intracellular domains of NLRR3 are indicated by open, gray and filled boxes, respectively. (C) Nuclear access of NLRR3-ICD. SK-N-BE cells were transfected with the expression plasmids encoding the above-mentioned HA-NLRR3 derivatives. Forty-eight hours after transfection, cells were fixed and stained with anti-HA antibody (red). Cell nuclei were stained with DAPI (blue). Scale bar; 10 μm. (D) Immunohistochemical staining. Human sympathetic ganglia were incubated with control IgG (left panel) or with anti-NLRR3 antibody (right panel). (For interpretation of the references to color in this figure legend, the reader is referred to the web version of this article.)

proteolytic processing, and thereby translocated from cell membrane to cell nucleus of cultured neuroblastoma cells as well as sympathetic ganglia.

3.4. NLRR3-ICD suppresses neuroblastoma cell proliferation

To explore a possible biological role(s) of NLRR3-ICD, we have examined the effect(s) of the indicated HA-NLRR3 derivatives including HA-NLRR3-ICD on neuroblastoma cell proliferation. SK-N-BE cells stably expressing the indicated HA-NLRR3 derivatives were cultured and their proliferation was monitored by IncuCyte live-cell imaging system. As shown in Fig. 4A, HA-NLRR3, HA-NLRR3-d-ECD and HA-NLRR3-ICD significantly suppressed SK-N-BE cell proliferation as compared with their parental cells. In a sharp contrast, HA-NLRR3-ECD and HA-NLRR3-ECD-sol had an undetectable effect on the rate of proliferation of SK-N-BE cells.

To further evaluate these observations, we have performed colony formation assay. SK-N-BE cells transfected with the indicated HA-NLRR3 derivatives were transferred to the fresh medium containing G418 (600 μg/ml). Two weeks after selection, number of drug-resistant colonies was scored. As shown in Fig. 4B and C, overexpression of HA-NLRR3-d-ECD or HA-NLRR3-ICD resulted in a remarkable decrease in number of drug-resistant colonies as compared with the empty plasmid control cells, whereas HA-NLRR3-ECD and HA-NLRR3-ECD-sol had a marginal effect on number of drug-resistant colonies. Additionally, cells overexpressing HA-NLRR3 showed a modest decrease in the rate of colony formation. Similar results were also obtained in neuroblastoma TGW cells (data not shown). Thus, these results indicate that NLRR3-ICD potentially plays a crucial role in the regulation of neuroblastoma cell proliferation.

3.5. NLRR3-ICD stimulates ATRA-mediated neuroblastoma cell differentiation

Since SH-SY5Y cells showed the remarkable ATRA-induced neurite extension accompanied by the massive accumulation of NLRR3-ICD (Fig. 1A), it is possible that NLRR3-ICD has a capability to trigger or enhance neurite elongation in neuroblastoma cells initiated by ATRA. To address this issue, SK-N-BE cells stably expressing the indicated NLRR3 derivatives were exposed to 1.5 μM of ATRA. Five days after treatment, images were taken and then total neurite outgrowth was assessed. As shown in Fig. 4D and E, an obvious increase in number of cells with neurite extension was observed in HA-NLRR3, HA-NLRR3-d-ECD or HA-NLRR3-ICD-expressing cells relative to that in the empty plasmid control cells. In contrast, HA-NLRR3-ECD and HA-NLRR3-ECD-sol did not have a significant effect on ATRA-mediated neurite outgrowth. Similar

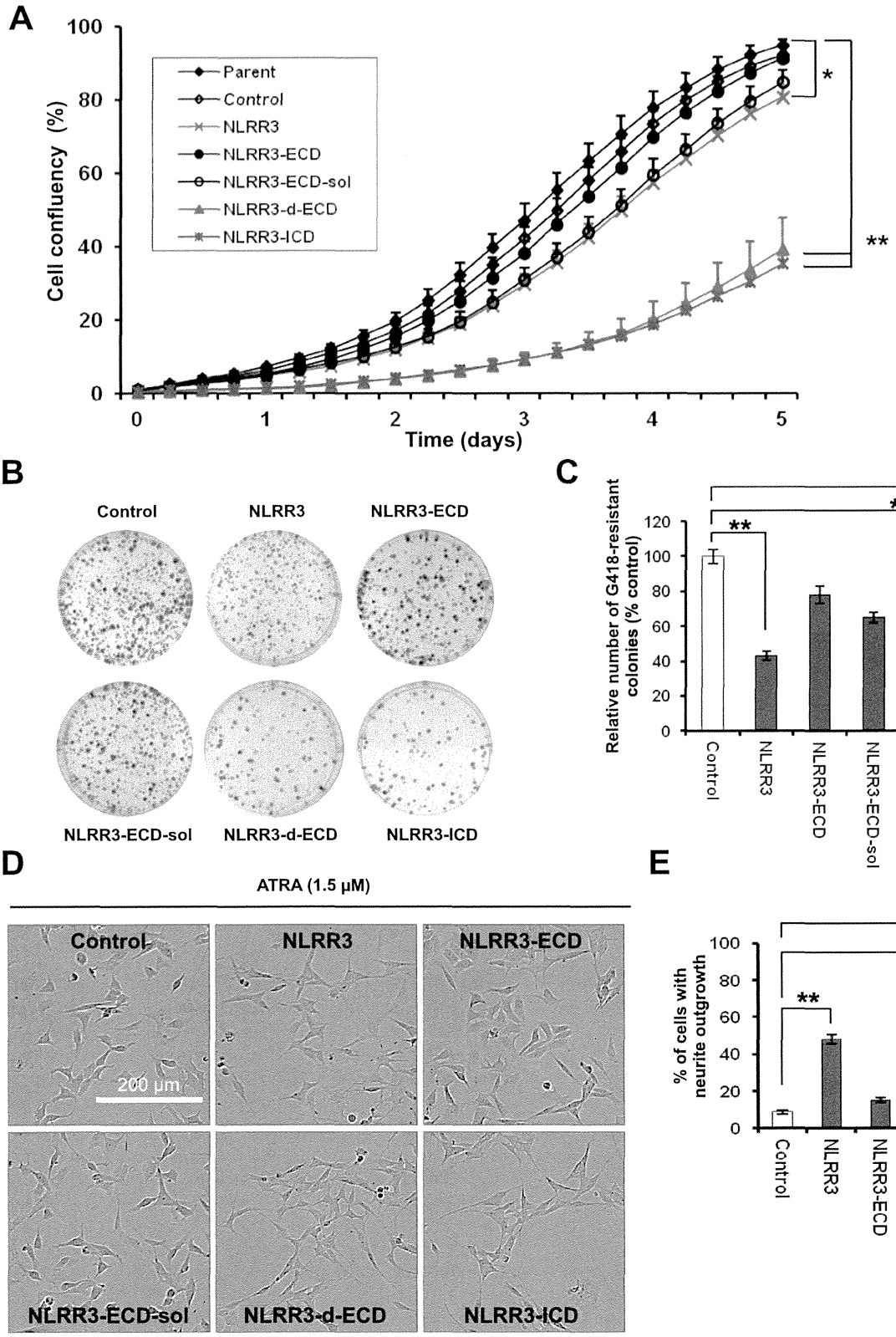

Fig. 4. NLRR3-ICD promotes growth suppression and ATRA-dependent neurite extension of neuroblastoma cells. (A) Growth curves. SK-N-BE cells stably expressing the indicated NLRR3 derivatives were grown in the medium and their growth rates were monitored by IncuCyte. (B and C) Colony formation assay. SK-N-BE cells were transfected with the indicated expression plasmids, and maintained in the culture medium containing 600 μg/ml of G418. Two weeks after the selection, drug-resistant colonies were stained with Giemsa's solution (B) and scored (C). (D and E) NLRR3-ICD enhances neurite elongation in response to ATRA. SK-N-BE cells stably expressing the indicated NLRR3 derivatives were maintained in the culture medium containing 1.5 μM of ATRA for 5 days and their images were taken through phase-contrast microscope. Scale bar; 200 μm (D). Histogram illustrates the percentage of neurite-bearing cells (E).

results were also obtained in the immunostaining experiments using anti-Tuj-1 antibody (Supplementary Fig. S1). Collectively, our present findings strongly suggest that the secretase-mediated proteolytic processing of NLRR3 to generate the COOH-terminal intracellular fragment and its subsequent nuclear access play a pivotal role in the regulation of ATRA-dependent neuroblastoma differentiation.

4. Discussion

It has been well-recognized that the therapeutic approach based on the induced differentiation of tumor cells is one of the most attractive strategies for malignant and aggressive tumor treatment. In this connection, a growing body of evidence demonstrated that retinoids have an ability to induce neuronal differentiation of neuroblastoma [19]. Indeed, ATRA-mediated differentiation of neuroblastoma cells has become a currently used therapeutic protocol. However, a precise molecular basis behind the neuroblastoma differentiation following ATRA exposure has been elusive. In this study, we have found for the first time that NLRR3, which is expressed higher in favorable neuroblastomas relative to unfavorable ones, participates in ATRA-induced neuroblastoma differentiation, and thus our present results might provide a novel insight into understanding ATRA-mediated biological responses such as differentiation.

One of the interesting findings of the present study is that the COOH-terminal intracellular domain of NLRR3 (NLRR3-ICD) is induced to be released from the plasma membrane and then accumulates in cell nucleus during ATRA-dependent differentiation of neuroblastoma SH-SY5Y cells. Indeed, ATRA-mediated nuclear access of NLRR3 in SH-SY5Y cells was massively attenuated in the presence of γ-secretase inhibitor as examined by immunostaining experiments (data not shown), and NLRR3-ICD production was significantly blocked by α- or γ-secretase inhibitor treatment, suggesting that ATRA-induced generation of NLRR3-ICD is regulated at least in part by secretase activities. In accordance with the previous findings showing that there are no distinct consensus amino acid sequences of intramembrane γ-cleavage sites among a broad range of its substrates [16], NLRR3 transmembrane domain also displayed no amino acid sequence similarity to those of Notch as well as the other γ-secretase substrates. However, the transmembrane domain of NLRR3 was highly conserved among human, mouse and rat (Fig. 2A), raising a possibility that γ-secretase-mediated liberation of the intracellular cytoplasmic domain of NLRR3 is evolutionarily conserved across mammalian species.

Meanwhile, it has been well-known that the released NICD directly moves from cytoplasm to nucleus, and then forms nuclear transcription complex with the sequence-specific DNA-binding protein CSL, Mastermind (MAM) family of transcriptional co-activators and/or transcriptional co-repressor MINT to transactivate and/or transrepress Notch-target genes [15]. According to our present observations, the exogenously expressed HA-NLRR3-ICD was translocated to cell nucleus, and also HA-NLRR3-ICD generated in SK-N-BE cells overexpressing HA-NLRR3 was detectable in nuclear fraction. Since we found out a canonical nuclear translocation signal (NLS) within NLRR3-ICD (RNYLQKPTFALGELYPP), it is possible that the nuclear access of NLRR3-ICD might be mediated by this putative NLS. Considering that Notch signaling results in the up-regulation and/or down-regulation of various Notch-target gene expression, it should be critical to investigate whether, like NICD, NLRR3-ICD could form active transcription complexes to regulate its target gene expression implicated in ATRA-mediated neuroblastoma differentiation.

As described [14], NLRR family consists of three members including NLRR1, NLRR2 and NLRR3. The close inspection of their transmembrane domains showed that there is no amino acid sequence similarity among them. Although a biological significance(s) of NLRR2 has remained to be determined, we have demonstrated that, in contrast to NLRR3, NLRR1 is expressed higher in unfavorable neuroblastomas as compared with that in favorable ones, and its expression level is correlated with poor prognosis of patients with neuroblastoma [13]. Subsequent studies revealed that *NLRR1* is a direct transcriptional target of MYCN and has an oncogenic potential [20]. Notably, there existed an inverse relationship between the expression levels of *NLRR3* and *MYCN* during ATRA-mediated neuroblastoma differentiation [14]. In support with this notion, forced expression and siRNA-mediated knockdown of *MYCN* resulted in a massive down- and up-regulation of *NLRR3* expression, respectively [14]. Based on our observations, it is likely that NLRR family such as NLRR1 and NLRR3 stands at the crossroad between MYCN-mediated oncogenic transformation and neuronal differentiation. Further studies should be required to adequately address this issue.

Taken together, our present findings strongly suggest that NLRR3-ICD generated by secretase-mediated proteolytic processing of NLRR3 contributes to ATRA-induced neuroblastoma differentiation, and might provide a clue to develop a novel therapeutic strategy for the treatment of aggressive neuroblastoma based on ATRA-induced differentiation.

Acknowledgments

This work was supported by a Grant-in-Aid from the Japan Ministry of Health, Labour and Welfare for Third Term Comprehensive Control Research for Cancer to A.N., JSPS KAKENHI Grant Number 21390317, 24249061 to A.N., 19890276 to A.T., MEXT KAKENHI Grant Number 22791016 to A.T.

Appendix A. Supplementary data

Supplementary data associated with this article can be found, in the online version, at http://dx.doi.org/10.1016/j.bbrc.2014.09.065.

References

[1] J.M. Maris, Recent advances in neuroblastoma, N. Engl. J. Med. 362 (2010) 2202–2211.
[2] G.M. Brodeur, A. Nakagawara, Molecular basis of clinical heterogeneity in neuroblastoma, Am. J. Pediatr. Hematol. Oncol. 14 (1992) 111–116.
[3] M.J. Cooper, S.M. Steinberg, J. Chatten, A.E. Evans, M.A. Israel, Plasticity of neuroblastoma tumor cells to differentiate along a fetal adrenal ganglionic lineage predicts for improved patient survival, J. Clin. Invest. 90 (1992) 2402–2408.
[4] A. Nakagawara, M. Arima-Nakagawara, N.J. Scavarda, C.G. Azar, B. Cantor, G.M. Brodeur, Association between high levels of expression of the TRK gene and favorable outcome in human neuroblastoma, N. Engl. J. Med. 328 (1993) 847–854.
[5] V.R. Ganeshan, N.F. Schor, Pharmacologic management of high-risk neuroblastoma in children, Paediatr. Drugs 13 (2011) 245–255.
[6] J. Hara, Development of treatment strategies for advanced neuroblastoma, Int. J. Clin. Oncol. 17 (2012) 196–203.
[7] D. Meitar, S.E. Crawford, A.W. Rademaker, S.L. Cohn, Tumor angiogenesis correlates with metastatic disease, N-myc amplification, and poor outcome in human neuroblastoma, J. Clin. Oncol. 14 (1996) 405–414.
[8] J.M. Maris, K.K. Matthay, Molecular biology of neuroblastoma, J. Clin. Oncol. 17 (1999) 2264–2279.
[9] G.P. Tonini, Neuroblastoma: the result of multistep transformation?, Stem Cells 11 (1993) 276–282
[10] R. Ijiri, Y. Tanaka, K. Kato, K. Misugi, H. Nishihira, Y. Toyoda, H. Kigasawa, T. Nishi, M. Takeuchi, N. Aida, T. Momoi, Clinicopathologic study of mass-screened neuroblastoma with special emphasis on untreated observed cases: a possible histologic clue to tumor regression, Am. J. Surg. Pathol. 24 (2000) 807–815.
[11] G. López-Carballo, L. Moreno, S. Masiá, P. Pérez, D. Barettino, Activation of the phosphatidylinositol 3-kinase/Akt signaling pathway by retinoic acid is required for neural differentiation of SH-SY5Y human neuroblastoma cells, J. Biol. Chem. 277 (2002) 25297–25304.
[12] M. Ohira, A. Morohashi, H. Inuzuka, T. Shishikura, T. Kawamoto, H. Kageyama, Y. Nakamura, E. Isogai, H. Takayasu, S. Sakiyama, Y. Suzuki, S. Sugano, T. Goto, S. Sato, A. Nakagawara, Expression profiling and characterization of 4200

genes cloned from primary neuroblastomas: identification of 305 genes differentially expressed between favorable and unfavorable subsets, Oncogene 22 (2003) 5525–5536.
[13] S. Hamano, M. Ohira, E. Isogai, K. Nakada, A. Nakagawara, Identification of novel human neuronal leucine-rich repeat (hNLRR) family genes and inverse association of expression of Nbla10449/hNLRR-1 and Nbla10677/hNLRR-3 with the prognosis of primary neuroblastomas, Int. J. Oncol. 24 (2004) 1457–1466.
[14] J. Akter, A. Takatori, M.S. Hossain, T. Ozaki, A. Nakazawa, M. Ohira, Y. Suenaga, A. Nakagawara, Expression of NLRR3 orphan receptor gene is negatively regulated by MYCN and Miz-1, and its downregulation is associated with unfavorable outcome in neuroblastoma, Clin. Cancer Res. 17 (2011) 6681–6692.
[15] K. Hori, A. Sen, S. Artavanis-Tsakonas, Notch signaling at a glance, J. Cell Sci. 126 (2013) 2135–2140.
[16] B. De Strooper, Aph-1, Pen-2, and Nicastrin with Presenilin generate an active gamma-Secretase complex, Neuron 38 (2003) 9–12.
[17] G.H. Searfoss, W.H. Jordan, D.O. Calligaro, E.J. Galbreath, L.M. Schirtzinger, B.R. Berridge, H. Gao, M.A. Higgins, P.C. May, T.P. Ryan, Adipsin, a biomarker of gastrointestinal toxicity mediated by a functional gamma-secretase inhibitor, J. Biol. Chem. 278 (2003) 46107–46116.
[18] S.E. Hoey, R.J. Williams, M.S. Perkinton, Synaptic NMDA receptor activation stimulates alpha-secretase amyloid precursor protein processing and inhibits amyloid-beta production, J. Neurosci. 29 (2009) 4442–4460.
[19] M. Ponzoni, P. Bocca, V. Chiesa, A. Decensi, V. Pistoia, L. Raffaghello, C. Rozzo, P.G. Montaldo, Differential effects of N-(4-hydroxyphenyl)retinamide and retinoic acid on neuroblastoma cells: apoptosis versus differentiation, Cancer Res. 55 (1995) 853–861.
[20] M.S. Hossain, T. Ozaki, H. Wang, A. Nakagawa, H. Takenobu, M. Ohira, T. Kamijo, A. Nakagawara, N-MYC promotes cell proliferation through a direct transactivation of neuronal leucine-rich repeat protein-1 (NLRR1) gene in neuroblastoma, Oncogene 27 (2008) 6075–6082.

Cancer Science
Japanese Cancer Association JCA
Open Access

Identification of a novel E-box binding pyrrole-imidazole polyamide inhibiting MYC-driven cell proliferation

Rajeev Mishra,[1,2] Takayoshi Watanabe,[1,3] Makoto T. Kimura,[1] Nobuko Koshikawa,[3] Maki Ikeda,[1] Shota Uekusa,[1] Hiroyuki Kawashima,[1,4] Xiaofei Wang,[1] Jun Igarashi,[1] Diptiman Choudhury,[2] Carla Grandori,[5] Christopher J. Kemp,[5] Miki Ohira,[3] Narendra K. Verma,[6] Yujin Kobayashi,[7] Jin Takeuchi,[7] Tsugumichi Koshinaga,[4] Norimichi Nemoto,[8] Noboru Fukuda,[9] Masayoshi Soma,[10] Takeshi Kusafuka,[4] Kyoko Fujiwara[10] and Hiroki Nagase[1,3]

[1]Division of Cancer Genetics, Department of Advanced Medical Science, Nihon University Research Institute of Medical Science, Tokyo, Japan; [2]Department of Medicine, Cedars-Sinai Medical Center, Samuel Oschin Comprehensive Cancer Institute, Los Angeles, California, USA; [3]Chiba Cancer Center Research Institute, Chiba; [4]Division of Pediatric Surgery, Department of Surgery, Nihon University Research Institute of Medical Science, Tokyo, Japan; [5]Division of Human Biology, Fred Hutchinson Cancer Research Center, Seattle, Washington, USA; [6]Department of Biological Sciences, Padova University, Padova, Italy; [7]Division of Hematology, Department of Internal Medicine, Nihon University Research Institute of Medical Science, Tokyo; [8]Department of Pathology and Microbiology, Nihon University Research Institute of Medical Science, Tokyo; [9]Life Science, Advanced Research Institute for the Sciences and Humanities, Nihon University, Tokyo; [10]Innovative Therapy Research Group, Nihon University Research Institute of Medical Science, Tokyo, Japan

Key words

Cell cycle, E-Box, MYC, pyrrole-imidazole polyamide, transcription therapy

Correspondence

Hiroki Nagase, Chiba Cancer Center Research Institute, 666-2 Nitona-cho, Chuo-ku, Chiba 260-8717, Japan.
Tel: +81-43-264-5431; Fax: +81-43-263-8175;
E-mail: hnagase@chiba-cc.jp

Funding information

Ministry of Education, Culture, Sports, Science and Technology of Japan (#23300344). (#26290060). Setsuro Fujii Memorial Osaka Foundation for the Promotion of Fundamental Medical Research, Osaka. National Institutes of Health/National Institute of Environmental Health Science North Carolina, USA. (R01 ES012249).

Received October 30, 2014; Revised January 9, 2015; Accepted January 11, 2015

Cancer Sci (2015)

doi: 10.1111/cas.12610

The MYC transcription factor plays a crucial role in the regulation of cell cycle progression, apoptosis, angiogenesis, and cellular transformation. Due to its oncogenic activities and overexpression in a majority of human cancers, it is an interesting target for novel drug therapies. MYC binding to the E-box (5′-CACGTGT-3′) sequence at gene promoters contributes to more than 4000 MYC-dependent transcripts. Owing to its importance in MYC regulation, we designed a novel sequence-specific DNA-binding pyrrole–imidazole (PI) polyamide, Myc-5, that recognizes the E-box consensus sequence. Bioinformatics analysis revealed that the Myc-5 binding sequence appeared in 5′- MYC binding E-box sequences at the eIF4G1, CCND1, and CDK4 gene promoters. Furthermore, ChIP coupled with detection by quantitative PCR indicated that Myc-5 has the ability to inhibit MYC binding at the target gene promoters and thus cause downregulation at the mRNA level and protein expression of its target genes in human Burkitt's lymphoma model cell line, P493.6, carrying an inducible MYC repression system and the K562 (human chronic myelogenous leukemia) cell line. Single i.v. injection of Myc-5 at 7.5 mg/kg dose caused significant tumor growth inhibition in a MYC-dependent tumor xenograft model without evidence of toxicity. We report here a compelling rationale for the identification of a PI polyamide that inhibits a part of E-box-mediated MYC downstream gene expression and is a model for showing that phenotype-associated MYC downstream gene targets consequently inhibit MYC-dependent tumor growth.

The transcription factor c-MYC possesses an exclusive and extensive set of biological actions that underlie its role as a salient oncogene and therefore could be the key to anticancer drug development. The c-MYC proto-oncogene belongs to the family of MYC genes that includes B-MYC, L-MYC, N-MYC, and S-MYC.[1] Among them, c-MYC (here after referred as MYC) is found in almost all proliferating cells and expression of N- and L-MYC is more constrained to specific cell types.[2] MYC is a basic helix–loop–helix leucine zipper transcription factor that binds DNA in a sequence-specific manner[3] and activates the transcription of genes whose products are involved in crucial aspects of cancer biology such as cell proliferation, cell growth, apoptosis, and differentiation.[4] The biological activities of MYC depends on its ability to heterodimerize with its protein partner, MAX, to bind the enhancer box (E-box) sequence and stimulate transcription of a number of its downstream genes.[4,5] The MAX:MAX homodimer or MAD:MAX heterodimer is supposed to antagonize the functions of MYC by binding to the same core E-box sequences.[6]

MYC targets approximately 10–15% of all cellular promoters in human cells, which is higher than any other typical transcription factor.[7] Target genes of MYC identified in mammalian cells include genes involved in cell cycle, ribosomal biogenesis, protein synthesis, and mitochondrial function.[4,5,8] Among the direct target genes of MYC, those with E-box binding sites include *ODC*, *ECA39*, *eIF4E*, *CDC25*, *CAD*, *CDK4*, *eIF4G1*, and *CCND1*.[9,10] MYC has been known to play a crucial role in malignant transformation.[11] Several attempts have been made using small molecule inhibitors to inhibit MYC binding at gene promoters.[11–15] Pyrrole–imidazole (PI) polyamides are a class of sequence-specific DNA-binding small molecules that have been shown to be effective inhibitors of transcription factors by disrupting essential

protein–DNA interactions.[16–20] Our group and others have designed PI polyamides to specifically target critical regulatory proteins, including MMP-9, transforming growth factor-β1, vascular endothelial growth factor, hypoxia-inducible factor 1-α, androgen receptor, epidermal growth factor receptor, prostate-specific antigen, and lectin-type oxidized LDL receptor-1.[16,21–24] Recently, we have demonstrated that E-Box recognizing PI polyamide, Myc-6 was found to significantly suppress malignant phenotypes of human osteosarcoma MG63 cells both *in vitro* and *in vivo*, showing the potential of PI polyamides in cancer therapy.[25]

In the present study, we developed an E-box-binding PI polyamide, Myc-5 (target sequence 5′-WCWCGWGW-3′, where W = A or T) to inhibit MYC target genes. Myc-5 showed inhibition of MYC-driven cell growth by downregulation of a subgroup of MYC downstream genes, including *eIF4GI* and *CCND1*, at an early stage of transcription. In animal tumor model studies, Myc-5 inhibits tumor growth by inhibiting cell proliferation and inducing apoptosis in tumor tissue. Collectively, our results establish a transcriptional regulation at an early stage of MYC regulatory proteins by using PI polyamides and provide a novel antitumor agent targeting MYC function.

Materials and Methods

Cell culture. The human Burkitt's lymphoma model cell line, P493.6, carrying Tet-repressible c-MYC system and chronic myeloid leukemia cell line K562, were used in this study. To suppress MYC expression, P493.6 cells were treated with 0.1 μg/mL tetracycline for 3 days before treatment with Myc-5. The P493.6 cell line was kindly provided by C. Grandori (Fred Hutchinson Cancer Research Center, Seattle, WA, USA) and K562 cells were obtained from the Riken cell bank (Ibaraki, Japan).

Synthesis of PI polyamides targeting the E-box consensus sequence. Myc-5 was designed to target the E-box consensus sequence and mismatch PI polyamide was designed to target by exchanging the CG dinucleotide with GC in the center of the E-box (Fig. 1a,c). Fluorescein isothiocyanate-conjugated Myc-5 was also synthesized for nuclear localization experiments (Fig. 1b). All of the PI polyamides were synthesized according to previously established methods.[21]

Electrophoretic mobility shift assay and surface plasmon resonance. FITC-labeled matching hairpin oligonucleotide (46 base pair) corresponding to eIF4G1 gene promoters having E-box consensus binding sites and mismatch promoter were synthesized (Table S1) for EMSA. Results were visualized by luminescent image analyzer LAS3000 (Fujifilm, Tokyo, Japan). The kinetic measurements of the polyamides' binding curves to the biotin-labeled double-stranded DNA (having the E-box consensus sequence) and data processing were carried out on a Biacore 2000 system as described previously.[26]

Quantitative real-time PCR. Total RNA was extracted and digested with DNase I using the RNeasy kit according to the manufacturer's protocol (Qiagen, Valencia, CA, USA). The primer sequences are listed in Table S2. Relative gene expression was determined by normalizing the gene expression of each target gene to *GAPDH*.

Conventional ChIP followed by real-time PCR. The status of polyamide binding at the target promoter region (Table S3) was detected using a ChIP assay kit (Upstate Biotechnology, Upstate Biotechnology, Inc., Lake Placid, NY, USA) following the manufacturer's protocol. ChIP DNA was further analyzed by quantitative PCR using primers encompassing the regions of interest on the eIF4G1, CCND1, and CDK4 promoters.

Tumorigenicity studies in SCID mice. Seven-week-old SCID mice were housed under specific pathogen-free conditions. Experiments were approved by the committee for laboratory animal welfare and ethics of Nihon University School of Medicine (Tokyo, Japan). The effect of Myc-5 on the xenograft model was examined as follows. P493.6 cells (1×10^7) were inoculated s.c. into the flank of mice and they were divided into three treatment groups: control group (PBS i.v.; $n = 8$); a Myc-5 treated group (7.5 mg/kg i.v., single dose; $n = 8$); and a doxycycline treated group (0.01% doxycycline in regular

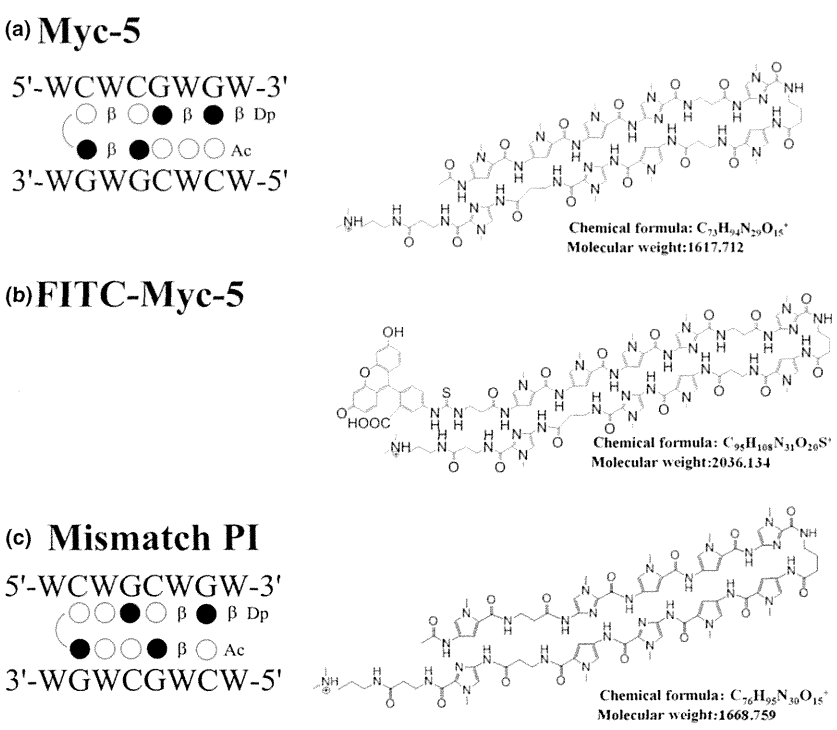

Fig. 1. Designed pyrrole–imidazole (PI) polyamide structure and binding site. Structures and binding sites for synthesized PI polyamides Myc-5 (a), FITC-labeled Myc-5 (b), and mismatch PI polyamide (c). Base sequence specificity depends on side-by-side pairing of pyrrole and imidazole amino acids in the minor groove of DNA. Black and white circles represent imidazole and pyrrole rings, respectively; curved lines represent hairpin junctions. β, β-alanine; Dp, diaminomethylene propylamide; W, A or T.

drinking water; $n = 5$). Doxycycline induces repression of P493.6 xenograft tumor growth in a MYC-dependent manner. The treatment was started on day 7 after cell inoculation and mice were killed after 30 days of treatment.

***In vivo* nuclear localization.** For *in vivo* nuclear localization analysis by fluorescence microscopy, tumor-bearing mice were injected with FITC-labeled Myc-5 (0.15 mg) into the lateral tail vein of the animals. Tumor tissues, along with adjacent normal tissues, were collected 5 days after the injection for analysis using propidium iodide as a nuclear dye to identify nucleated cells.

Statistical analysis. Results are shown as mean ± SD. Each experiment was carried out independently three times. The level of significance ($^{**}P < 0.05$ and $^{***}P < 0.001$) was determined using Student's *t*-test.

Additional supplementary materials and methods detailing cell viability assay, detection of nuclear localization by confocal microscopy, histopathology, Western blot analysis, microarray analyses, and references can be found in Documents S1 and S2.

Results

Identification of MYC target genes that harbor Myc-5 consensus sequence. E-boxes are present in many genes, but not all are known to be direct transcriptional targets of MYC. Based on compilations by Fernandez *et al.*,[27] we found that 105 genes harbor the Myc-5 binding site (WCWCGWGW) in their E-box consensus sequence (Table S4). These genes can be classified into a wide range of functional classes. Here we focused on genes related to translation and proliferation. Among the ten top MYC-regulated genes we chose two proliferation genes (*CDK4* and *CCND1*) and a translation gene (*eIF4G1*). The selected genes have been well characterized by previous researchers and are also well known direct targets of MYC.[9,10,28]

DNA-binding affinity and specificity of designed Myc-5 PI polyamide. The EMSA and surface plasmon resonance (SPR) assay are used to determine the binding affinity and specificity of PI polyamide to its target DNA. The EMSA results demonstrated that a clear mobility band shift (Fig. 2a,b) was detected when Myc-5 was incubated with eIF4G1 gene promoter oligonucleotide, whereas no shift was detected for the mismatch PI polyamide (Fig. 2a, lane 4) or eIF4G1 mismatch gene promoter (Fig. 2a, lane 5) in which the core recognition sequence, CACGTG, was replaced by CAGCTG. Increasing concentrations of Myc-5, but not of the mismatch PI polyamide, bound to the eIF4G1 promoter oligo (Fig. 2b, lanes 2–5), suggesting that Myc-5 can specifically bind to sequences of their target gene-promoters. To further confirm binding of the E-box to

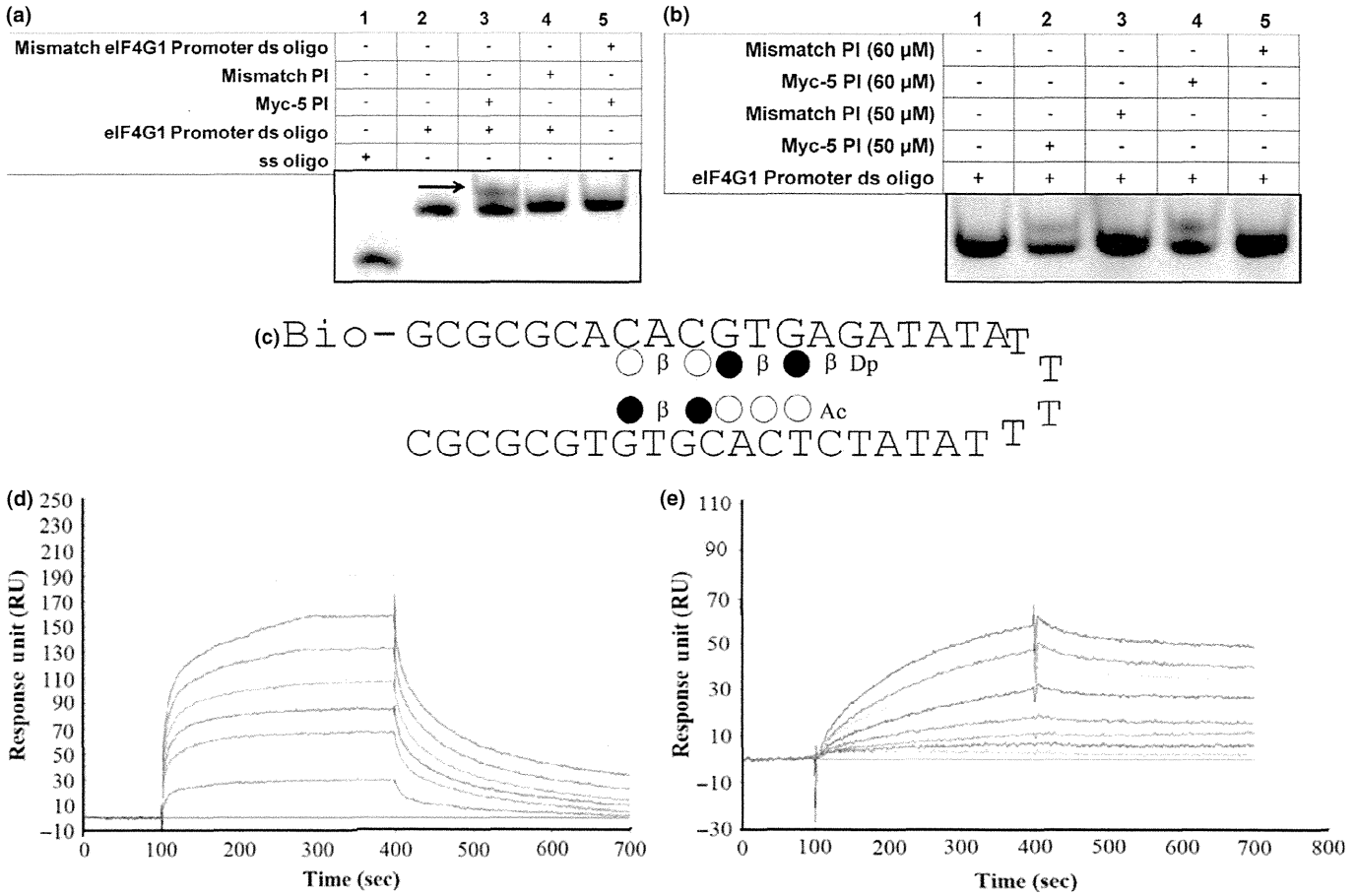

Fig. 2. Myc-5 binding at the target gene promoters. (a) EMSA of *eIF4G1* gene match and mismatch promoter and with Myc-5 and mismatch pyrrole–imidazole (PI) polyamide. (b) EMSA of *eIF4G1* gene promoter with Myc-5 and mismatch PI polyamide. FITC-labeled hairpin oligonucleotide was incubated at 37°C for 60 min in Myc-5 or mismatch PI polyamide. (c) Typical surface plasmon resonance sensograms for the interaction between PI polyamides and the hairpin duplex with 5′-biotin labeled and immobilized E-box (CACGTG) sequences. (d, e) Remarkable differences in binding kinetics were observed: fast on/off kinetics for Myc-5 (d), and slower kinetics for the mismatch PI polyamide (e).

the target gene promoter, we used a biosensor-SPR assay to explore the interaction of Myc-5 with biotinylated hairpin duplexes having WCWCGWGW sequences (Fig. 2c). The kinetic profile of Myc-5 revealed a relatively fast "on-rate" and slow "off-rate" in binding with a K_D of $4.81 \pm 2.79 \times 10^{-8}$ M. The mismatch PI polyamide showed slow "on-rate" and fast "off-rate" with K_D was calculated at $5.1 \pm 0.54 \times 10^{-5}$. In summary, these results confirm that the presence of the E-box in the DNA sequence has a pronounced influence on the binding of Myc-5 and yields a 654-times higher affinity than the mismatch PI polyamide (Fig. 2d,e, Table S5).

Myc-5 inhibited cell proliferation and localized into nucleus in P493.6 and K562 cell lines. P493.6 and K562 cells were incubated with different concentrations (1–10 μM) of Myc-5 and mismatch PI polyamide and viability was determined at 24, 48, and 72 h after treatment, respectively. As shown in Figure S1, cell viability was significantly reduced ($P < 0.001$ *vs* control) in both cell lines treated with Myc-5 in a time- and concentration-dependent manner. Nuclear localization of Myc-5 was determined by FITC-conjugated Myc-5 using laser confocal fluorescence microscopy. Green fluorescence indicates the presence of Myc-5 and red fluorescence depicts the cell nuclei, indicating that Myc-5 localizes into nuclei within 2 h (Fig. S2a,c,d). In contrast, cells incubated with FITC solution (control) at the same concentration did not localize into nuclei (Fig. S2b) in either cell line.

Myc-5 attenuates MYC binding at the gene promoter, causing downregulation of MYC target genes. Myc-5 inhibited target gene expression at protein and mRNA levels (Fig. 3a,b). Cells treated with Myc-5 at 10 μM concentration for 72 h caused statistically significant suppression of eIF4G1 mRNA compared with control or mismatch PI polyamide treated cells in both systems. The CCND1 mRNA was unaffected in

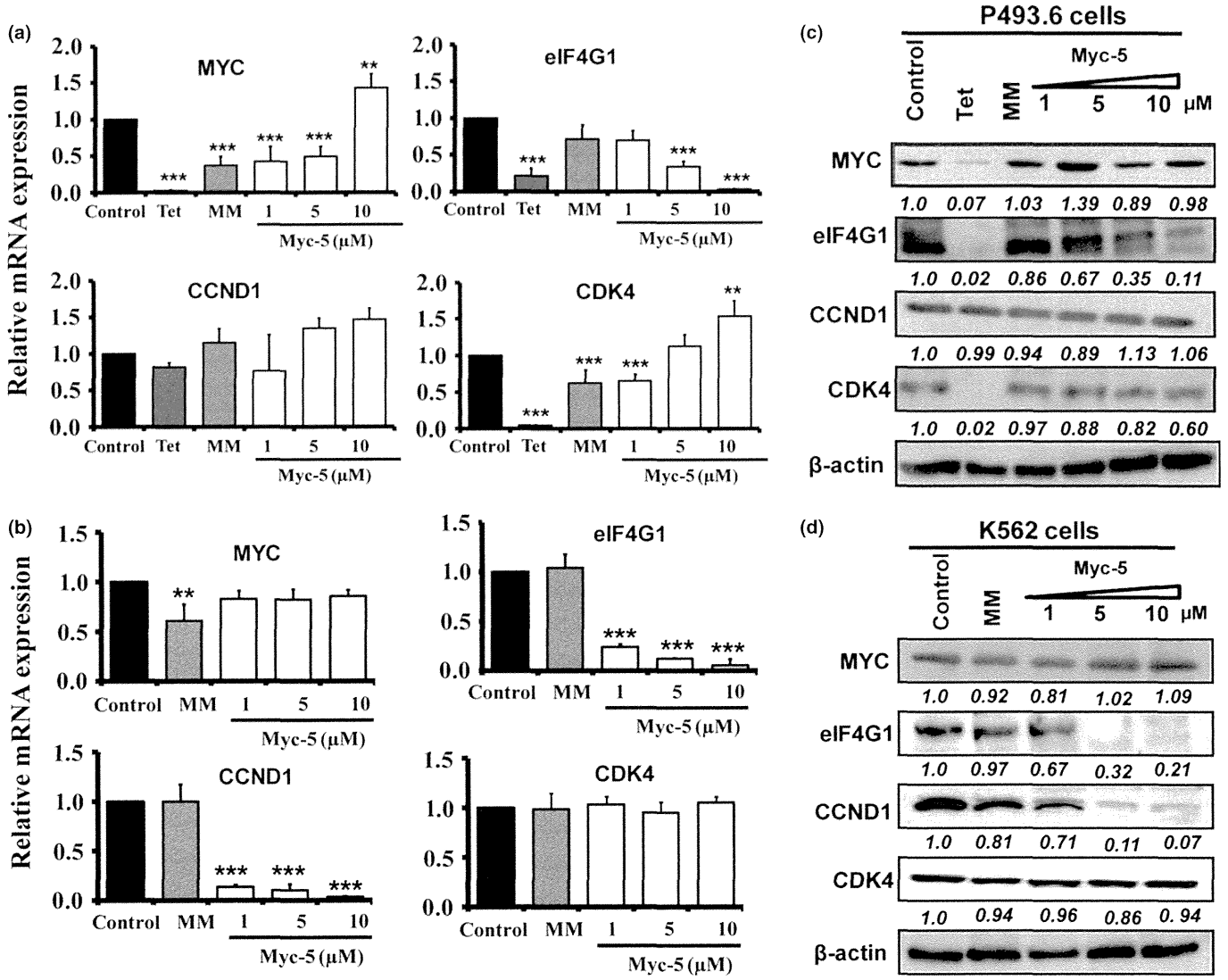

Fig. 3. Myc-5 downregulates mRNA expression and protein expression of target genes. (a, b) Expression of target genes was detected by quantitative real-time PCR after 72 h of treatment with control, Myc-5 (1, 5, and 10 μM concentration), or mismatch PI polyamide (MM) at 10 μM concentration and normalized with GAPDH in P493.6 (a) and K562 (b) cells. Data are shown as mean values with error bars representing ±SD. Statistical significance was calculated by Student's *t*-test. $^{**}P < 0.05$, $^{***}P < 0.001$ when compared to control. (c, d) P493.6 and K562 cells were treated with Myc-5 (1, 5, and 10 μM) or mismatch PI polyamide (10 μM; MM) for 72 h. β-actin was used as the loading control. The relative band intensities in P493.6 and K562 cells were determined by dividing the intensity of the band by β-actin followed by normalization to the control. Tet, tetracycline.

all treated and untreated groups of P493.6 cells; however, its expression was significantly ($P < 0.001$) downregulated in the K562 cell line compared to control and mismatch PI polyamide treated groups. The mRNA expression correlated well with protein expression in the Myc-5 administration using both cell systems (Fig. 3c,d). To investigate whether target gene expression is directly regulated by Myc-5, we used ChIP assays of the E-box and exonic region (Figs 4a,b, S3a). The exonic region was taken as an arbitrary negative control region during the analysis. The ChIP analysis revealed that, compared to control, the Myc-5 and tetracycline groups significantly inhibited binding of MYC to the E-box region in P493.6 cells (Figs 4c,S3b) at the eIF4G1 and CDK4 gene promoters. In contrast, the E-box and control regions (exon) of CCND1 gene promoter showed restrained enrichment in all treated groups (Fig. 4d). Similarly, MYC was specifically enriched near the E-box site at the eIF4G1, CCND1, and CDK4 gene promoters but not in the Myc-5 treated group in K562 cells (Figs 4e,f,S3c). Moreover, our microarray analysis results showed (Fig. S4a,b) that differentially expressed genes in K562 cells (29 upregulated and 21 downregulated) and P943.6 cells (20 genes upregulated and 20 downregulated) were identified by unpaired two-class significance analysis of microarray with 0% false discovery rate. Among the top 50 modulated genes, five were carrying the Myc-5 consensus sequence in their promoter, as identified from Table S4.

Myc-5 retards growth in animal tumor models. To investigate whether the *in vitro* efficacy of Myc-5 can also be recapitulated *in vivo*, therapeutic animal studies were carried out using P493.6 s.c. xenografts. Mice were inoculated s.c. with P493.6 (high MYC expressing) cells. One week after inoculating the cells, when the tumor volumes reached approximately 100 mm^3, mice were split into three groups and treated with either saline, doxycycline, or 7.5 mg/kg Myc-5 injected i.v. into the lateral tail vein of animals at day 7 (single dose; Fig. 5a). Myc-5 was formulated based on previous xenograft studies with PI polyamide.[20,29,30] Growth curve data indicated that Myc-5 (7.5 mg/kg) and doxycycline treated groups had a significantly smaller tumor volume during the growth phase ($P < 0.001$ *vs* control; Fig. 5b) by the end of the study. Representative images of each group of mice are shown in Fig. 5b (inset). All mice with Myc-5 treatment continued to gain weight at an equal rate throughout the treatment period (Fig. 5c). The average tumor weight results further confirmed inhibition of tumor growth as Myc-5 and doxycycline treated groups

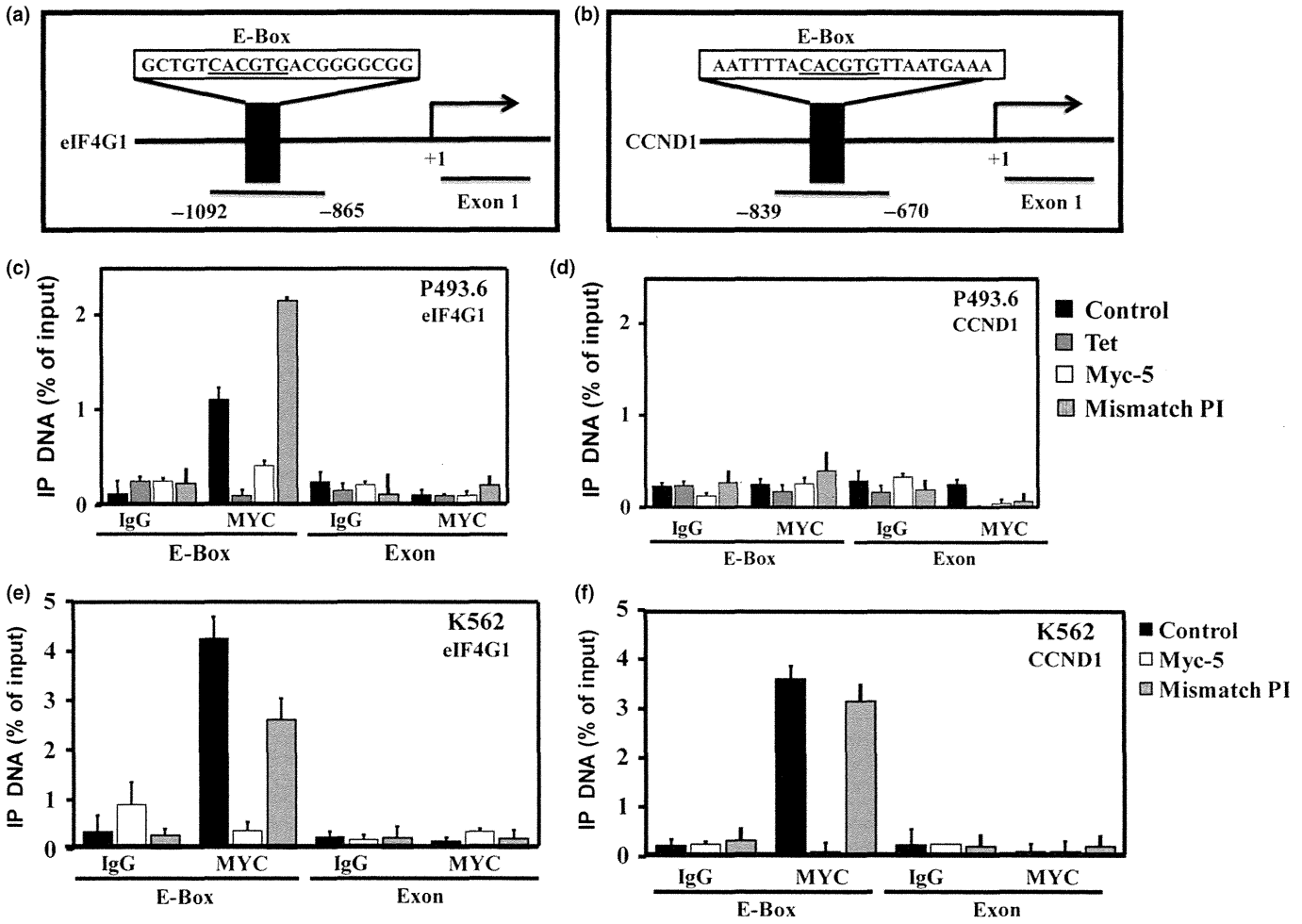

Fig. 4. *In vivo* binding of Myc-5 to the E-box at its target gene promoter. (a, b) Schematic depiction of the Myc-5 target gene promoter with MYC binding site (underline) indicated. (c–f) ChIP assay of Myc-5 target genes in the P493.6 (c, d) and K562 (e, f) cell systems. Labeled regions (E-box and exon) of each gene were quantitatively amplified by real-time PCR. Data are representative of three independent experiments. Tet, tetracycline.

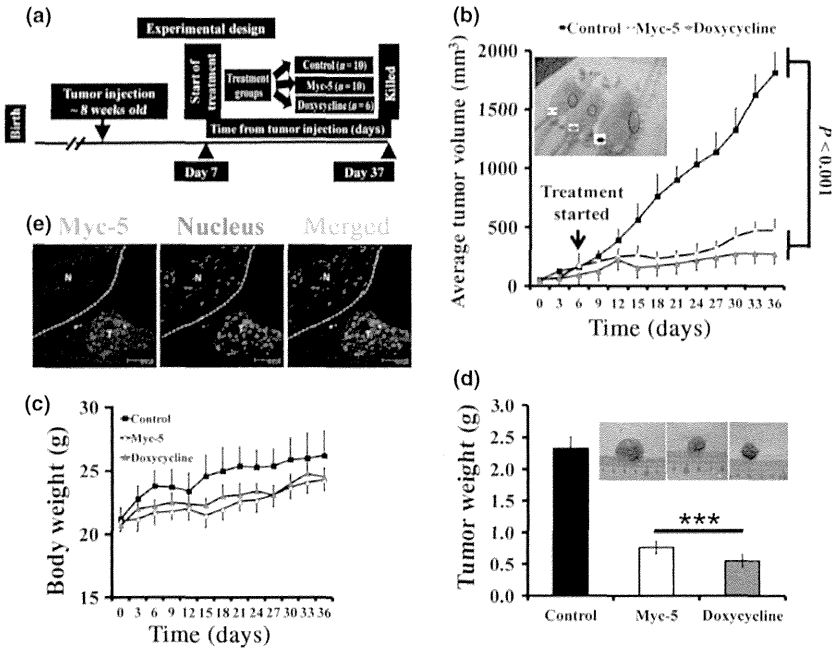

Fig. 5. Myc-5 blocks the growth of P493.6 xenografts. (a) Schematic diagram of the xenograft model illustrating timing of tumor implantation and treatment. Eight-week-old SCID mice were s.c. injected with P493.6 cells. (b) Tumor growth chart showing the effect of treatment *in vivo*. Myc-5 (7.5 mg/kg) and doxycycline significantly slowed tumor growth ($P < 0.001$) at the termination point in comparison to the control group. Representative picture shows each group of mice (inset). (c) Mean body weight for each treatment group plotted as function of day after post-injection. (e) Comparisons of excised tumor weights for three different treatment groups at the end of study. Data in (b, d, e) are shown as the mean ± SD. Statistical significance was calculated by Student's *t*-test. ***$P < 0.001$. (e) FITC-labeled Myc-5 localizes to nucleus of P493.6 xenograft leaving normal tissue unaffected (separated by white line). N: Normal tissue, T: tumor tissue.

were found to be significantly lower ($P < 0.001$ *vs* control; Fig. 5d) at the termination of the study.

Myc-5 localizes into tumor and causes decreased cell proliferation and induced apoptosis in P493.6 tumor xenografts. To evaluate *in vivo* nuclear localization, single i.v. injection of FITC-conjugated Myc-5 was given to P493.6 cell-derived xenografts. Twenty-four hours after injection, animals were killed and tumor tissues were obtained. The tumor-derived tissues were found to display strong and characteristic nuclear staining (Fig. 5e). In contrast, adjacent normal tissues were found to be devoid of nuclear fluorescence (Fig. 5e). Myc-5 was found throughout the tumor, indicating its capacity to enter the tumor through the vascular system. To assess the activity of Myc-5, tumors were harvested from all treatment groups and examined by histopathology. Microscopic analysis of H&E staining showed that Myc-5 and doxycycline treated tumors showed areas with necrosis, cellular debris, and swollen cells with cytoplasmic vacuoles as compared with the vehicle-treated control (Fig. 6a; left). In order to investigate the mechanism underlying Myc-5-mediated tumor growth inhibition in P493.6 xenografts, immunohistochemical analyses were carried out for BrdU uptake, and TUNEL reaction assay. BrdU-positive nuclei were detected in a small number of cells in Myc-5 treated tumor as compared to control group (Fig 6a; middle). In contrast, a large number of cells stained positively for TUNEL in Myc-5 or doxycycline treated group (Fig. 6a; right) compared to the control group. Quantitative data were consistent with the expression pattern of BrdU and TUNEL staining assays (Fig. 6b). Quantification of BrdU-positive cells in the control group were significantly ($P < 0.001$) reduced (approximately 83% and 76% reductions in Myc-5 and doxycycline groups, respectively) compared to treated groups. The TUNEL analysis showed that the number of apoptotic cells was significantly higher ($P < 0.001$; approximately 38% and 30% higher in Myc-5 and doxycycline groups, respectively) in treated groups. Overall, we found that Myc-5 is well tolerated, inhibits tumor growth, and induces apoptosis in P493.6 xenograft mouse models.

Discussion

In this study, we synthesized two β-alanine-linked polyamides of different lengths: Myc-5 (AcPyPyPyImβImγPyβPyImβImβDp), where Py is pyrrole, Im is imidazole, Ac is acetyl, β is β-alanine, Dp is dimethylaminopropylamine, and γ is γ-*turn* to target the 8-bp site of 5′-WCWCGWGW-3′; and mismatch polyamide (AcPyβImPyPyImγPyPyImPyβImβDp) to target the 8-bp site 5′-WCWGCWGW-3′, flipping dinucleotide CG to GC at the central portion (Fig. 1a,b). A search for Myc-5-binding sites from the published database[27] revealed that the Myc-5 consensus sequence was flanking the E-box of genes involved in apoptosis, cell cycle, nucleolar function, ribosomal proteins, and translation initiation factors. Among them, we focused on the *eIF4G1*, *CCND1*, and *CDK4* genes because they carry a Myc-5 consensus sequence including a MYC binding site (E-box) in the promoter region (Fig. S3d) and their transcription is modulated by MYC.[9,10,28] Using EMSA and Biacore analyses, our results showed that Myc-5 binds specifically and with high affinity (654 times; Table S5) to the eIF4G1, CCND1, and CDK4 gene promoters at the E-box region (Fig. 2). The effective concentration of Myc-5 in the EMSA was higher than the concentration for biological effect, which is consistent with results obtained for other compounds;[31] possibly, PI polyamide accumulates in cells to effectively reach the intracellular and intranuclear levels.[32] The higher binding affinity of Myc-5 in comparison to mismatch PI polyamide might be explained as the targeted PI polyamide has more aliphatic

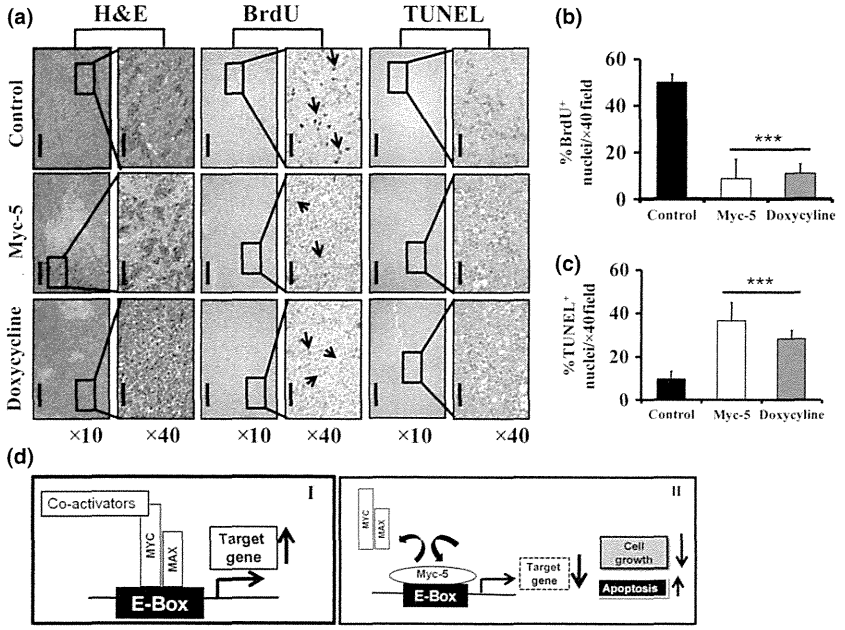

Fig. 6. Histopathology of xenografts in nude mice and illustration of potential mechanism by Myc-5. (a) Tissue sample were analyzed qualitatively for morphological changes. Magnification, ×10 (scale bar = 200 μm); magnification, ×40 (scale bar = 50 μm). (b, c) Quantitative data of immunohistochemical analysis of BrdU and TUNEL positive staining in each group. Data in (b, c) are shown as the mean ± SD of three tumor samples from an individual mouse in each group. Statistical significance was calculated by Student's *t*-test. ***$P < 0.001$. (d) Schematic diagram of the mechanism by which pyrrole–imidazole polyamide inhibits MYC/MAX interaction to the E-box. (I) MYC:MAX dimer binds to E-box and activates MYC target gene expression. (II) Myc-5 occupied the E-box by binding, thereby inhibiting the MYC/MAX interaction to the E-box, causing further suppression of target gene expression.

β-alanine unit, giving it more flexibility and optimizing the positioning of the imidazole amino acids on binding to its targeted sequence.[33] *In vivo* binding of Myc-5 to their target gene-promoter was confirmed by ChIP assay. Results of ChIP indicated that MYC transcription factor bound E-box in the control group whereas, in treated groups, Myc-5 inhibited MYC binding on its target gene promoters. However, in the P493.6 cell line, the CCND1 gene-promoter showed only a background signal that was obtained at the E-box region as well as in the control (exon) regions (Fig. 4d). These results were consistent with previous reports of the absence of this regulator in the B cell line.[34]

Myc-5 was used at the concentration of 10 μM based on previous studies using PI polyamides.[19,20,35] Myc-5 significantly reduced mRNA and protein expression of MYC target genes at this given concentration. The correlation between MYC binding and mRNA expression of Myc-5 was established by real-time mRNA expression analysis and Western blot analysis. The *eIF4G1* gene has a downregulated expression and might be a direct target of MYC in both systems, which was also favored by EMSA and ChIP data. CCND1 mRNA expression was downregulated in the K562 cell line with Myc-5 treatment in a dose-dependent manner, which is known to exert positive growth effects and to be regulated by MYC.[36] The mRNA expression of *CDK4*, a positive growth controller of MYC,[28] was unaffected by Myc-5 treatment as the Myc-5 binding site (E-box#2) has no role in MYC-dependent gene regulation.[28] We analyzed the CDK4 promoter region for putative MYC binding sites. Our sequence analysis revealed the presence of four E-box sequences, which could be recognized by MYC (Fig. S2). Among them, only E-box#2 is a putative binding site for Myc-5 as it contains the Myc-5 consensus sequence. As shown in Figure S2, Myc-5 bound to the E-box#2 of the CDK4 promoter. The *CDK4* gene is established as a direct target of MYC identified by serial analysis of gene expression with essential E-boxes in their promoters.[28] The CDK4 promoter contains four highly conserved E-box elements where E-box#3 and #4 were the most important for CDK4 promoter activity.[28] The Myc-5 effect on mRNA expression of the MYC gene and further its transcriptional target genes were analyzed by real-time PCR in K562 and P493.6 cell lines. In K562 cells, MYC mRNA expression is unaffected by Myc-5 treatment and a similar trend was observed in its target gene CDK4 mRNA expression. However MYC mRNA expression in Myc-5 treated group is significantly increased as compared to control group in P493.6 cells. P493.6 B lymphoma cells overexpress MYC, which indicates that P493.6 cell lines may have some mutations on its promoter or regulator regions. The MYC promoter or regulatory regions do not have any Myc-5 binding consensus sequence. This may be due to some specific mutation in these regions that might have generated a novel Myc-5 binding site at the MYC promoter of P493.6 cells. This novel Myc-5 binding site in the promoter could be acting as a transcriptional activator of the MYC gene and helping it to further overexpress. Furthermore, Myc-5 has very high affinity for its consensus sequence and may act as a non-competitive inhibitor of MYC protein. Therefore, overexpression of MYC protein in P493.6 cells does not have an effect on MYC downstream genes with active Myc-5 binding sites, such as eIF4G1.

Taken together, our data are compatible with a mechanism that involves the recruitment of Myc-5 at E-box sites within the promoter of the MYC target gene, thereby inhibiting MYC binding at particular sites and inhibiting target gene function instead of blocking MYC. Myc-5 downregulates its target gene transcription, supporting the notion that polyamides bind to DNA with affinity and sequence-specificity comparable to DNA-binding proteins and gene expression can be regulated

by competitive displacement of transcription factor from DNA target sequences,[37] where Myc-5 consensus sequences are not contained.

Myc-5 exerts its therapeutic role in tumor maintenance through selective effects on the translation of specific downstream genes. In our *in vivo* study we used 7.5 mg/kg on the basis of prior pharmacokinetic profiles and previous analytical studies.[20,38] We identified strong *in vivo* nuclear localization of Myc-5 and also its inhibitory effect on tumor growth in a P493.6 mouse model. One possible reason for this activity can be explained by previous reports showing that changes in the levels or activity of eIF4F mediate the translational regulation of specific genes involved (as in the P493.6 cell line, eIF4G1 is completely suppressed) in survival and apoptosis.[39] In nasopharyngeal carcinoma, knockdown of eIF4G1 expression markedly inhibited cell-cycle progression, proliferation, and suppressed *in vivo* xenograft tumor growth,[40,41] which might be applicable to our system as well.

In conclusion, the results reported here identify a novel PI polyamide, Myc-5, as a lead compound targeting against the E-box and thereby modulating expression of some genes. Our approach can be an efficient tool to identify the sequence-specific compound that targets the E-box and specifically modulates MYC downstream genes and interferes with their pathways. Myc-5 competes with the MYC:MAX heterodimer and inhibits transregulation of the target gene promoter (Fig. 6d) at the E-box. The extension of this approach could result in the identification of more potent inhibitory PI polyamides in multiple pathways and reveal a new E-box-regulated target or combination of targets for a distinct MYC function, which may have formidable therapeutic opportunities for the future.

Acknowledgments

We thank Mr. Shigeki Nakai, Ms. Asako Oguni, Mr. Motoaki Kataba, Ms. Yuki Yamada, and Ms.Yukari Obana, for their technical support and Ms. Paula Jones, Dr. Manisha Tripathi, and Dr. Sandrine Billet for critical reading. This work was supported by the Academic Frontier Project for 2006 Project for Private Universities, a matching fund subsidy and Grant-in-Aid for Scientific Research (B) (#23300344 and #26290060) from the Ministry of Education, Culture, Sports, Science and Technology of Japan (to H. Nagase), the Setsuro Fujii Memorial, and the Osaka Foundation for the Promotion of Fundamental Medical Research, Osaka (to H. Nagase). Support was also received from the Nihon University Strategic Projects for Academic Research and R01 ES012249 from the National Institutes of Health/National Institute of Environmental Health Science, North Carolina, USA. (to H. Nagase).

Disclosure Statement

The authors have no conflict of interest.

References

1 Adhikary S, Eilers M. Transcriptional regulation and transformation by Myc proteins. *Nat Rev Mol Cell Biol* 2005; **6**: 635–45.
2 Luscher B. Function and regulation of the transcription factors of the Myc /Max/Mad network. *Gene* 2001; **277**: 1–14.
3 Blackwood EM, Eisenman RN. Max: a helix-loop-helix zipper protein that forms a sequence-specific DNA-binding complex with Myc. *Science* 1991; **251**: 1211–7.
4 Dang CV, O'Donnell KA, Zeller KI *et al.* The c-Myc target gene network. *Semin Cancer Biol* 2006; **16**: 253–64.
5 Liu YC, Li F, Handler J *et al.* Global regulation of nucleotide biosynthetic genes by c-Myc. *PLoS One* 2008; **3**: e2722.
6 Ayer DE, Eisenman RN. A switch from Myc: Max to Mad: Max heterocomplexes accompanies monocyte/macrophage differentiation. *Genes Dev* 1993; **7**: 2110–9.
7 Guccione E, Martinato F, Finocchiaro G *et al.* Myc-binding-site recognition in the human genome is determined by chromatin context. *Nat Cell Biol* 2006; **8**: 764–70.
8 Zeller KI, Jegga AG, Aronow BJ *et al.* An integrated database of genes responsive to the Myc oncogenic transcription factor: identification of direct genomic targets. *Genome Biol* 2003; **4**: R69.
9 Huerta M, Munoz R, Tapia R *et al.* Cyclin D1 is transcriptionally down-regulated by ZO-2 via an E box and the transcription factor c-Myc. *Mol Biol Cell* 2007; **18**: 4826–36.
10 Lin CJ, Cencic R, Mills JR *et al.* c-Myc and eIF4F are components of a feedforward loop that links transcription and translation. *Cancer Res* 2008; **68**: 5326–34.
11 Albihn A, Johnsen JI, Henriksson MA. MYC in oncogenesis and as a target for cancer therapies. *Adv Cancer Res* 2010; **107**: 163–224.
12 Wang H, Chauhan J, Hu A *et al.* Disruption of Myc-Max heterodimerization with improved cell-penetrating analogs of the small molecule 10074-G5. *Oncotarget* 2013; **4**: 936–47.
13 Wang H, Hammoudeh DI, Follis AV *et al.* Improved low molecular weight Myc-Max inhibitors. *Mol Cancer Ther* 2007; **6**: 2399–408.
14 Yin X, Giap C, Lazo JS *et al.* Low molecular weight inhibitors of Myc-Max interaction and function. *Oncogene* 2003; **22**: 6151–9.
15 Delmore JE, Issa GC, Lemieux ME *et al.* BET bromodomain inhibition as a therapeutic strategy to target c-Myc. *Cell* 2011; **146**: 904–17.
16 Dervan PB, Doss RM, Marques MA. Programmable DNA binding oligomers for control of transcription. *Curr Med Chem Anticancer Agents* 2005; **5**: 373–87.
17 Dickinson LA, Burnett R, Melander C *et al.* Arresting cancer proliferation by small-molecule gene regulation. *Chem Biol* 2004; **11**: 1583–94.
18 Nickols NG, Szablowski JO, Hargrove AE *et al.* Activity of a py-im polyamide targeted to the estrogen response element. *Mol Cancer Ther* 2013; **12**: 675–84.
19 Yang F, Nickols NG, Li BC *et al.* Antitumor activity of a pyrrole-imidazole polyamide. *Proc Natl Acad Sci U S A* 2013; **110**: 1863–8.
20 Raskatov JA, Nickols NG, Hargrove AE *et al.* Gene expression changes in a tumor xenograft by a pyrrole-imidazole polyamide. *Proc Natl Acad Sci U S A* 2012; **109**: 16041–5.
21 Wang X, Nagase H, Watanabe T *et al.* Inhibition of MMP-9 transcription and suppression of tumor metastasis by pyrrole-imidazole polyamide. *Cancer Sci* 2010; **101**: 759–66.
22 Nickols NG, Jacobs CS, Farkas ME *et al.* Modulating hypoxia-inducible transcription by disrupting the HIF-1-DNA interface. *ACS Chem Biol* 2007; **2**: 561–71.
23 Matsuda H, Fukuda N, Ueno T *et al.* Transcriptional inhibition of progressive renal disease by gene silencing pyrrole-imidazole polyamide targeting of the transforming growth factor-beta1 promoter. *Kidney Int* 2011; **79**: 46–56.
24 Kang JS, Meier JL, Dervan PB. Design of sequence-specific DNA binding molecules for DNA methyltransferase inhibition. *J Am Chem Soc* 2014; **136**: 3687–94.
25 Taniguchi M, Fujiwara K, Nakai Y *et al.* Inhibition of malignant phenotypes of human osteosarcoma cells by a gene silencer, a pyrrole-imidazole polyamide, which targets an E-box motif. *FEBS Open Bio* 2014; **4**: 328–34.
26 Chen M, Matsuda H, Wang L *et al.* Pretranscriptional regulation of Tgf-beta1 by PI polyamide prevents scarring and accelerates wound healing of the cornea after exposure to alkali. *Mol Ther* 2010; **18**: 519–27.
27 Fernandez PC, Frank SR, Wang L *et al.* Genomic targets of the human c-Myc protein. *Genes Dev* 2003; **17**: 1115–29.
28 Hermeking H, Rago C, Schuhmacher M *et al.* Identification of CDK4 as a target of c-MYC. *Proc Natl Acad Sci U S A* 2000; **97**: 2229–34.
29 Chou CJ, Farkas ME, Tsai SM *et al.* Small molecules targeting histone H4 as potential therapeutics for chronic myelogenous leukemia. *Mol Cancer Ther* 2008; **7**: 769–78.
30 Chou CJ, O'Hare T, Lefebvre S *et al.* Growth arrest of BCR-ABL positive cells with a sequence-specific polyamide-chlorambucil conjugate. *PLoS One* 2008; **3**: e3593.
31 Berg T, Cohen SB, Desharnais J *et al.* Small-molecule antagonists of Myc /Max dimerization inhibit Myc-induced transformation of chicken embryo fibroblasts. *Proc Natl Acad Sci U S A* 2002; **99**: 3830–5.
32 Yao EH, Fukuda N, Ueno T *et al.* A pyrrole-imidazole polyamide targeting transforming growth factor-beta1 inhibits restenosis and preserves endothelialization in the injured artery. *Cardiovasc Res* 2009; **81**: 797–804.
33 Farkas ME, Li BC, Dose C *et al.* DNA sequence selectivity of hairpin polyamide turn units. *Bioorg Med Chem Lett* 2009; **19**: 3919–23.

34 Arvanitakis L, Yaseen N, Sharma S. Latent membrane protein-1 induces cyclin D2 expression, pRb hyperphosphorylation, and loss of TGF-beta 1-mediated growth inhibition in EBV-positive B cells. *J Immunol* 1995; **155**: 1047–56.
35 Wang YD, Dziegielewski J, Wurtz NR *et al.* DNA crosslinking and biological activity of a hairpin polyamide-chlorambucil conjugate. *Nucleic Acids Res* 2003; **31**: 1208–15.
36 Mateyak MK, Obaya AJ, Sedivy JM. c-Myc regulates cyclin D-Cdk4 and -Cdk6 activity but affects cell cycle progression at multiple independent points. *Mol Cell Biol* 1999; **19**: 4672–83.
37 Nickols NG, Dervan PB. Suppression of androgen receptor-mediated gene expression by a sequence-specific DNA-binding polyamide. *Proc Natl Acad Sci U S A* 2007; **104**: 10418–23.
38 Synold TW, Xi B, Wu J *et al.* Single-dose pharmacokinetic and toxicity analysis of pyrrole-imidazole polyamides in mice. *Cancer Chemother Pharmacol* 2012; **70**: 617–25.
39 Li S, Perlman DM, Peterson MS *et al.* Translation initiation factor 4E blocks endoplasmic reticulum-mediated apoptosis. *J Biol Chem* 2004; **279**: 21312–7.
40 Tu L, Liu Z, He X *et al.* Over-expression of eukaryotic translation initiation factor 4 gamma 1 correlates with tumor progression and poor prognosis in nasopharyngeal carcinoma. *Mol Cancer* 2010; **9**: 78.
41 Lin CJ, Nasr Z, Premsrirut PK *et al.* Targeting synthetic lethal interactions between Myc and the eIF4F complex impedes tumorigenesis. *Cell Rep* 2012; **1**: 325–33.

Supporting Information

Additional supporting information may be found in the online version of this article:

Doc. S1. Supplementary materials and methods.

Doc. S2. Reference list.

Fig. S1. Antiproliferative effect of Myc-5.

Fig. S2. Myc-5 localizes into nucleus.

Fig. S3. *In vivo* binding of Myc-5 at CDK4 gene promoter.

Fig. S4. Heat map represents the functional annotated transcripts that are identified by unpaired two-class significance analysis of microarray analysis with a false discovery rate of 0% from cells treated with DMSO (control), mismatch polyamide, and Myc-5.

Table S1. FITC-labeled oligomer sequences designed for EMSA

Table S2. Primers used in quantitative RT-PCR

Table S3. Primers used for ChIP real-time PCR

Table S4. Promoter-associated E-box genes

Table S5. Kinetic constant for Myc-5 pyrrole–imidazole polyamide and mismatch binding